DESIGN AND OPTIMIZATION OF DIFFUSER FOR HORIZONTAL AXIS DIFFUSER AUGMENTED HYDRO-KINETIC TURBINE

Waleed Khalid

Supervisor: Dr. Salma Sherbaz

Master of Science

In
Computational Science and Engineering

RESEARCH CENTRE FOR MODELING & SIMULATION

NATIONAL UNIVERSITY OF SCIENCES AND

TECHNOLOGY

2019

DESIGN AND OPTIMIZATION OF DIFFUSER FOR HORIZONTAL AXIS DIFFUSER AUGMENTED HYDRO-KINETIC TURBINE

Waleed Khalid

172887

Supervisor: Dr Salma Sherbaz

Research Centre for Modeling & Simulation

A thesis submitted to the

National University of Sciences & Technology

In partial fulfillment of the requirement for the degree of

Master of Science

In

Computational Science and Engineering

2019

<u>STATEMENT OF ORIGINALITY</u>

I hereby certify that the work embodied in this thesis is the result of original research and has not been submitted for a higher degree to any other University or Institution.

Date	Waleed Khalid

Acknowledgements

First and foremost I would like to acknowledge Allah Almighty Who always helped me during my life.

For the successful accomplishment of thesis and research endeavor, I honestly appreciate the way I was always motivated and personal support of my Supervisor Dr. Salma Sherbaz. Without her academic guidance, technical support and encouragement this thesis would not have been possible.

I would also like to thank my GEC Members, who helped me a lot in finalizing this project within the limited time frame.

Abstract

The research on marine renewable energy technologies is underway around the globe due to the compelling reasons such as environment friendly nature, renewable, intermittent but predictable, security and diversity of supply, and limited social and environmental impacts. However, in Pakistan there is little awareness and appreciation of the potential of these technologies. Owing to grave energy crisis, these renewable energy resources are inevitable for Pakistan.

The hydrokinetic turbine utilizes the kinetic energy of flowing water for the power generation. The horizontal axis hydro-kinetic turbine (HAHT) is probably one of the most promising marine renewable energy technologies due to high-power output and economic viability. Since the power produced by the tidal turbine is directly proportional to the cube of incoming velocity, a small increase in the velocity will increase the power output significantly. Therefore, the power output of a conventional bare turbine can be further improved by enclosing it within a diffuser and accelerating the incoming flow.

The aim of this project is the design and optimization of a diffuser for horizontal axis hydrokinetic turbine application. The two-dimensional flat plate airfoil is used as benchmark and flow around the airfoil is simulated using the commercial CFD software Ansys Fluent16. Later, CFD analyses are carried out for baseline diffuser generated from the flat plate airfoil. The performance of this diffuser was optimized by achieving an optimum curved profile at the internal surface of the diffuser. Bezier curves parameterization and design of experiment (DOE) techniques are used for this purpose. The Response Surface Methodology (RSM) is used as a tool for optimization. It is observed that by finding the optimum set of input parameters, maximum velocity (at the diffuser throat) that can be achieved is 3.68 m/s. This means that an augmentation of 34.3% in the velocity can be achieved with an optimum diffuser in comparison to baseline diffuser.

Contents

List of Figures

List of Tables

CHAPTER 1

Introduction

1.1 Background

Fossil fuels have been considered as a major main energy source for the global economic engine. In one way or the other, nearly all the industries and domestic units rely on energy produced by fossil fuels. With ever-increasing population and urbanization; the burden on fossil fuels has equivalently been increasing and will continue to do so until viable alternates are available. The fossil fuels have also caused degradation of our environment. This damage to the global climate has reached an alarming point and its impact has already been felt in recent decades. Carbon dioxide (CO_2) is the major anthropogenic greenhouse gas (GHG). The contribution of CO_2 emissions from industrial processes and fossil fuel combustion accounted for about 76% of the total anthropogenic GHG emissions increase between 1970 and 2010 (as shown in Figure 1.1). Lately, the governments around the globe, with the cooperation of the UN and regulatory bodies, are paying an ever-increasing attention to the environmental issues associated with fossil fuels.
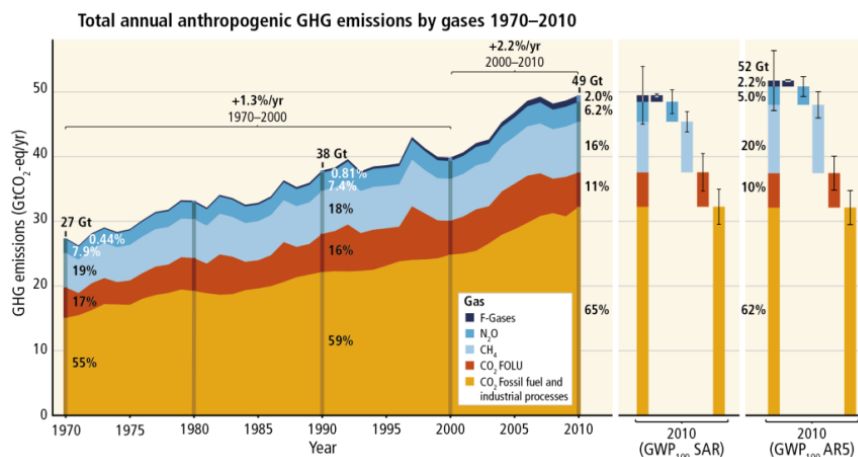
Figure 1. 1 Total annual anthropogenic greenhouse gas (GHG) emmissions (gigatone of CO2-equivalent per year, GtCO$_2$-eq/yr) for the period 1970 t0 2010, by gases [1]

The forecasted issues can only be resolved by shifting to alternate energy options having a lower carbon footprint. Ideally, these energy options are to be renewable in order to be sustainable in the longer run. Renewable energy sources, including, the sun, winds, water, biomass and geothermal, have shown significant promise in helping to reduce the amount of toxins produced by fossil fuel consumption [2].
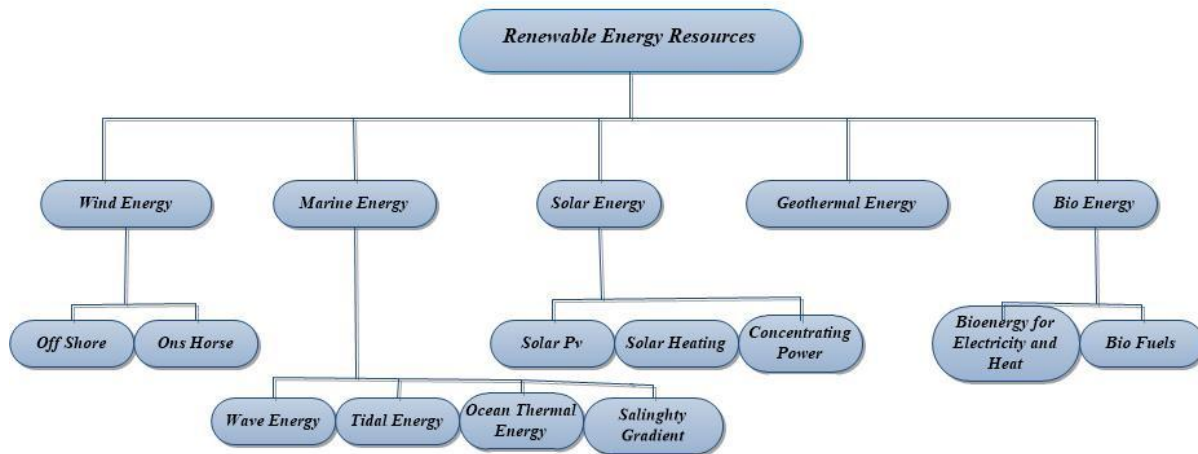
Figure 1. 2 Renewable energy resources

1.1.1   Marine Renewable Energy

Oceans are a great resource of vast untapped environment-friendly renewable energy. The sources for harnessing this marine renewable energy are divided in five different categories i.e. waves, tides, the difference in salinity gradients, and the heat stored in surface waters. A brief overview of these resources is given in the following paragraphs

1.1.1.1   Wave Energy

Wave energy converters (WECs) utilize the kinetic and potential energy of ocean waves to generate electricity. For the efficient extraction of wave energy, WECs can be located on the shoreline, near-shore, and offshore. Similarly, these devices can be installed independently as well as in the form of arrays to increase the power output [3-5]. The estimated amount of the wave energy that can be exploited with current technology is of order 29500 TWh/year [6].

1.1.1.2   Tidal Energy

Tides are the periodic rise and fall of sea level caused by the combined effects of the gravitational forces exerted by the sun and moon and the rotation of the earth. The working

principal of the tidal stream devices is similar to that of wind turbines and convert the kinetic energy of tidal currents into electricity. In addition, the owing to the higher density of the water, a tidal stream turbine can produce a potentially comparable amount of power with much smaller blades and low rotational speed. However, the cavitation at the tip of the turbine blades acts as an upper limit to the turbine rotational speed [7,8]. The Rance Tidal Power Station is the worlds' first tidal power plant located on the estuary of the Rance River in Brittany, France. This power plant has 24 turbine and 240 megawatts installed capacity [9].

The tidal energy conversion devices can be divided in six categories; horizontal axis turbines, vertical axis turbines, oscillating hydrofoil, venture effect tidal stream devices, Archimedes screw and tidal kite. A brief overview of these devices is given in the following paragraphs.

The horizontal axis turbines have two or three blades, a central hub and a shaft mounted horizontally parallel to the ground. The incoming flow creates a lift on the blades causing the rotor to turn. A generator then converts the spinning gear motion into electricity. In vertical axis turbines, the shaft is mounted on a vertical axis, normal to the ground [10, 11].

In reciprocating devices, a hydrofoil attached to an oscillating arm comes back and forth in a plane normal to the tidal stream. This motion then drives fluid in a hydraulic system to be converted into electricity [12]. In venture effect tidal stream devices, the incoming flow is accelerated by directing it through a duct/ shroud. The resulting pressure gradient force moves a conventional turbine inside the duct/ shroud [13].

A tidal kite consists of a small turbine mounted on a hydrofoil wing. The entire assembly is then tethered to the seabed. The incoming flow over the wing creates a lift force and pushes the kite in the forward direction. This results an increase in the speed of the flow passing through the turbine, generating a greater amounts of power using a smaller turbine [14,15].

1.1.1.3   Ocean Thermal Energy

Ocean thermal energy conversion (OTEC) is basically an energy generation technology using warm surface water and cold deep ocean water. The natural temperature gradient present in the oceans drives a heat engine. In OTEC, the temperature difference of at least 20° and ideally 30–40° is required for the maximum possible efficiency [16,17]. Active development in the area of

OTEC started in the 1970s and since then several OTEC plants have been successfully designed, constructed, and tested [18].
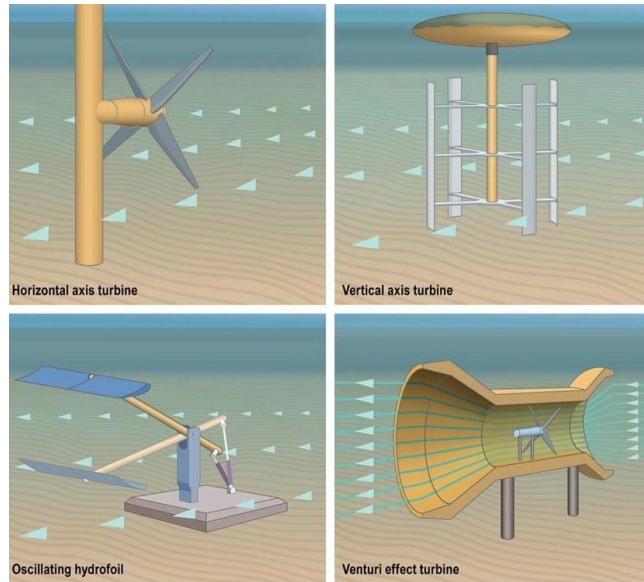
Figure 1. 3 Tidal energy conversion devices[18]

1.1.1.4   Salinity-Gradient Energy

Salinity-gradient energy, a potentially renewable and sustainable source of energy is the chemical energy associated with solvation of salts. Mixing two solutions of different concentration, releases Gibbs free energy. This energy can be used for the generation of electricity. Pressure retarded osmosis, reverse electro dialysis, and capacitive mixing are the main techniques used for salinity gradient energy generation [19, 20]. As per theoretical estimates, power that can be obtained from World's rivers discharge into the oceans is around 1.4–2.6 TW [21].

1.2   Area of Research

Horizontal axis hydrokinetic turbine (HAHT) is probably one of the most promising hydropower technologies due high power output per unit and economic viability [3, 21]. The power produced by the hydrokinetic turbine is directly proportional to the cube of incoming water velocity

(through the relation given in equation (1.1)) and a minor rise in the velocity will increase the power output significantly.

$$P = \frac{1}{2}A\rho v^3 \tag{1.1}$$

A is the area, ρ is the density of the flow and v is the velocity of the incoming flow and P is power.

Therefore the power output of a conventional bare turbine can be further improved by enclosing it within a diffuser, which accelerates the incoming flow. Since last decade, there has been increasing trend/ focus on diffuser augmented HAHT. The advantage is significant since this makes HAHT installation viable in regions with slow flow velocity and offers higher power output from already viable/operational sites. The aim of this project is the design and optimization of a diffuser for horizontal axis hydrokinetic turbine application.

1.3 Research Objectives

The main objectives are as follows:

- Design a diffuser to increase power output of hydrokinetic turbine using Computational Fluid Dynamic techniques.

- Optimize the diffuser design/ performance using computational fluid dynamics along with Bezier curves parameterization and response surface techniques

- CFD analysis of a diffuser augmented hydrokinetic turbine using actuator disk approach

1.4 Research Methodology

The aim of this study is the design and optimization of a diffuser using computational fluid dynamics techniques and is divided in three phases. In the first phase, the flat plate airfoil is taken as baseline geometry. The flow around the two-dimensional airfoil is simulated using the commercial CFD software Ansys Fluent. The numerically computed results are compared with the available data.

In the second phase, CFD analyses are carried out for baseline diffuser generated from the flat plate airfoil. Subsequently, performance of this diffuser was optimized by achieving an optimum

curved profile at the internal surface of the diffuser. Bezier curves parameterization and design of experiment (DOE) techniques are used for this purpose.

In the third phase, the performance of the optimized diffuser is analyzed using numerical actuator disc approach. The research methodology adopted in the current research is also illustrates in Figure 1.4.

Literature Review
- Problem definition
- Review of existing literature
- Identificatio of missing links/gaps

Bechmark Validation
- Flow simulation around the two-dimensional flatplate airfoil
- Comparision of simulated results with available data

Optimization of Diffuser Design / Performance
- CFD analyses of baseline diffuser generated from the flat plate airfoil
- Construction of different diffuser geometries using Bézier curves parameterization and design of experiment (DOE) techniques.
- CFD analyses of different diffuser geometries
- Identification of optimum diffuser using response surface methodology

Performance Analysis of Optimized Diffuser
- The performance analysis of optimized diffuser using numerical actuator disc approach.

Figure 1. 4 Research methodology

1.5   Contributions

The work done on diffuser augmented HAHT so far shows that the advantages of using a diffuser around the HAHT are recognized. There is an increasing trend/ focus on designing HAHT with diffusers. In this context, a number of NACA airfoils have been implemented/ investigated. The diffuser augmented HAHT has only been around for a little over a decade, so it is expected that the research work so far is still in establishing stage and mature approaches for diffuser design are under research, conceptualization or yet to come.

The missing part or next step is the realization that most of the diffuser design for HAHT applications so far, has been based on standard NACA airfoils. Although this work has generated

promising results, i.e. significant increase in power output. These airfoils are designed for high flow speed applications. Since the marine current velocity, most parts of the world, is almost 1 m/sec on average. The diffuser based on low flow speed hydrofoil will be ideal for HAHT applications.

The easiest starting point for this is existing airfoils designed for high lift low Reynolds number application. Starting with the geometry of this airfoil as a baseline, airfoil shape, after optimization, is used to generate the diffuser shape. The developed diffuser is further studied for suitability for HAHT applications using CFD techniques by examining the on-axis distribution of stream wise velocity and pressure coefficient.

1.6   Relevant Research in Pakistan

The proposed research a has enormous potential for Pakistan, which meets its energy requirements from conventional sources like Natural Gas 50% and Oil 30%20 and is facing a serious energy crisis. Pakistan possesses a large marine territory and finest network of natural streams and rivers. The research focused on diffuser augmented HAHT has enormous potential to contribute a substantial portion of the energy mix in Pakistan.

1.7   Organization of the Thesis

Chapter 1 --- Introduction

This chapter provides an introduction of marine renewable technologies. Research objectives and research methodology adopted for current study is also outlined.

Chapter 2 --- Literature Review

This chapter provides a brief overview of the research in the area of diffuser augmented HAHT.

Chapter 3---Mathematical Modeling

This chapter provides a brief overview of the mathematical model used for the design and optimization of diffuser and to analyze the performance of the diffuser augmented hydrokinetic turbines.

Chapter 4 --- Numerical Setup

This chapter includes of details of the numerical setup used in current study.

Chapter 5 --- Results and Discussion

This chapter provides a discussion of the main findings from the research.

Chapter 6 --- Conclusions and Future Work

Conclusions derived from the current research are presented. Recommendations for future efforts are also suggested in this chapter.

CHAPTER 2

Literature Review

Since last decade, there has been increasing trend/ focus on diffuser augmented HAHT. The advantage is significant since this makes HAHT installation viable in regions with slow flow velocity and offers higher power output from already viable/operational sites. This chapter provides a brief overview of the relevant studies conducted in the last fifteen years.

2.1   Background

Lawn used one-dimensional actuator disk theory to evaluate the performance of shrouded turbines.   The ducts present in upstream and downstream of the turbine were treated as contractions or expansions having specified diffusion efficiencies. It was observed that, for the case where the diffuser efficiency is constant, an optimum turbine resistance is required for generating maximum power. This is due to the fact that the swallowing capacity of the duct increases with decrease in resistance. It was also noticed that the controlled diffusion at the inlet has a very small impact in terms of power enhancements. On the other hand, efficient controlled diffusion at outlet resulted in 30 percent increase in the power coefficient of an optimized turbine [24].

Setoguchi et al. performed a detailed experimental investigation of a noval two-way diffuser for tidal turbine application. The two-way diffusers are believed to be the most suitable choice for the flow conditions involving the periodic changes in the direction of flow. The study also investigated the effects of the brim height and outside body shape on the performance of diffuser by measuring the pressure and velocity distribution along the central axis of the diffuser. The free stream velocity in case of the diffuser augmented turbine was reported to be 1.3 times more than that of bare turbine[25].

Kirke studied the effect of diffuser augmentation on the performance of a horizontal axis turbine. A 280 mm diameter axial flow turbine with various duct shapes was tested experimentally. A 70% increase in the output of the bare turbine was reported due to the use of a slotted diffuser (as shown in Figure 2.1) [26].
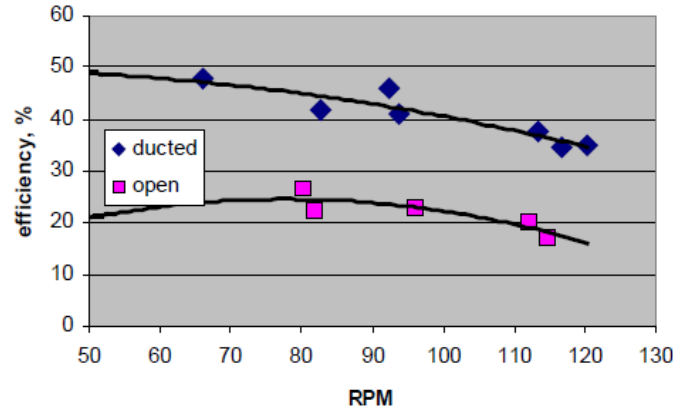
Figure 2. 1 Efficiency of a bare and diffuser augmented axial flow turbine[26]

Munch et al. assessed the performance of a ducted tidal turbine using unsteady turbulent flow simulation in open sea conditions. This study also involved the design and the optimization of a runner blade using element momentum theory. The purpose of this optimization was to improve the cavitation performance and reduce the maximum stress values and blade deformations. They also observed a significant increase the pressure drop and the fluid velocity through the rotor due to the duct arrangement [27].

Gaden and Bibeau performed a detailed investigation of the effect of diffuser in terms of enhancement in performance and viability of hydrokinetic turbines. The validated momentum source turbine model was used for turbine modeling. The power produced by the diffuser augmented turbine configuration was 3.1 times more than that of bare turbine. A scaling analysis was also used to demonstrate the improved performance of the diffuser augmented turbine compared to that of a larger size bare turbine [28].

Shives and Crawford simulated the flow around the various ducts designs using CFD based actuator disk technique. The main objective was to study the effect of various factors including viscous loss, flow separation and base pressure on the performance of ducts. It was concluded that effect of the viscous loss in the inlet area of the ducts had only a minor impact on the power whereas the base pressure effect gave a major improvement. Similarly, boundary layer flow separation in the diffuser section resulted in performance degradation [29].

20

The basic aim of the numerical study performed by Scherillo et al. was the design and performance evaluation of a shrouded hydro turbine. The whole assembly was also tested in the wind tunnel and a towing tank facility present at the University of Naples. A significant increase of the thrust was observed for the shrouded configurations. The increase in the power coefficient due shrouded turbine was about 7% [30].

Reinecke and Ventre studies a single curve plate diffuser with an area ratio of 3.29. In this study, the performed of diffuser augmented turbine and bare turbine is analyzed experimentally. The coefficient of maximum power (C_P) at a flow speed of 1.5ms^{-1} was found to be [1.74], whereas that of bare turbine was 0.43.[31]

Sun and Kyozuka investigated the effect of diffuser on the flow field around a turbine using CFD method and the blade element momentum (BEM) theory. Validation experiments for the both bare turbine and the shrouded turbine were conducted in the circulating water channel. The obtained results confirmed the positive effect of the brimmed diffuser from wind-lens technology on the performance of a tidal turbine. The power coefficient of the shrouded turbine was reported to be 2.5 times that of the bare turbine [32].
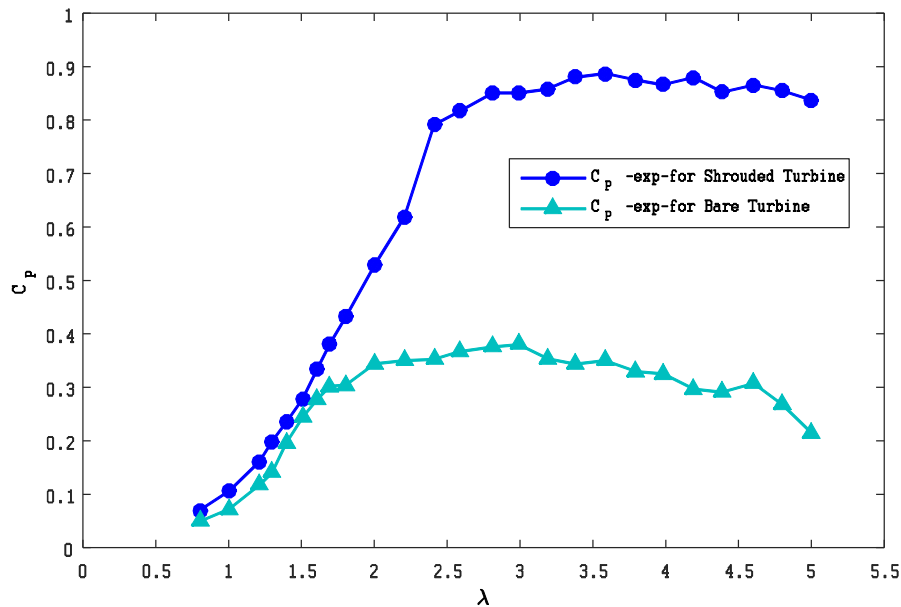
Figure 2. 2 Power coefficients for diffuser augmented and bare turbine [32].

Nasir et.al studied the effect of length and angle of NACA 0018 airfoil on the performance of diffuser using computational fluid dynamics techniques. The finite volume based CFD solver ANSYS Fluent was used for this purpose. An increase in the velocity of incoming flow at the diffuser throat was observed with increase in length and angle of attack. However the due to the flow separation after 14° angle of attack, velocity started to decrease. A similar trend was also observed in case of mass flow rate. [33]

The focus of the study conducted by Shi et.al was the designed and optimization of a thin-wall diffuser of a horizontal axis tidal turbine using computational fluid dynamics (CFD) methods and model testing. The two independent factors considered during the optimization study were the diffuser outlet diameter and expansion section length. The diffuser geometry was optimized to provide high flow acceleration ratio at the diffuser throat and minimum drag [34].

Khunthongjan and Janyalertadun studied the diffuser angle effect on the performance of the diffuser augmented turbine using one dimensional momentum theory and computational fluid dynamics (CFD) techniques. A significant augmentation in the velocity was observed for the diffuser angle between the 0-20° and 50-70° range [35].

The results of the numerical study conducted by. Shinomiya et al. confirmed the increase the efficiency of a conventional horizontal axis turbine due to the addition of diffuser. The flow around the four different diffuser geometries was simulated using finite volume method based software ANSYS – FLUENT. The computed numerical results were validated against the available experimental data. The results showed that the speed of the incoming flow in rotor plane of the diffuser augmented turbine was 1.5 times more than that of bare turbine [36].

Ait-Mohammed et al. observed a significant improvement in the hydrodynamic performance of a marine turbine due to the addition of a duct. The potential theory based panel method was used for this purpose. NACA 63-415 airfoil was used to design the blade profile of three bladed rotor turbine. The duct was designed using NACA4424 profile [37].

Ponta and Jacvkis [38] used three-dimensional Reynolds-averaged Navier-Stokes simulations to compare the performance of ducted and open center turbines. The whole study was divided in two phases. In the first phase, the turbine rotor was represented by a simple actuator, whereas In the second stage, the CFD-integrated blade element momentum is used for this purpose.

Chen and Zhou proposed the idea of a new marine current turbine with postpositive bulb geometry. The efficiency of this turbine was further enhanced by enclosing it within a diffuser. The flow around the bare and the diffuser augmented turbine was simulated numerically and validated with experimental data. A 3% increase in the speed of incoming flow at inlet reported due to the addition of the diffuser. A similar increase in the output power of the diffuser augmented turbine was also observed [39].

Shahsavarifard et al. reported the results of an experimental study performed on a 19.8 cm diameter horizontal axis hydrokinetic turbine with two different shrouds. The performance of the turbine with and without shroud was evaluated by measuring the power and thrust coefficients in each case. The maximum power coefficient of a shrouded turbine was found to be comparable with that of unshrouded one. It was observed that power generated by the bare turbine with an extended blade is same as that of shrouded turbine with a diameter equal to the diameter of the shroud exit [40].
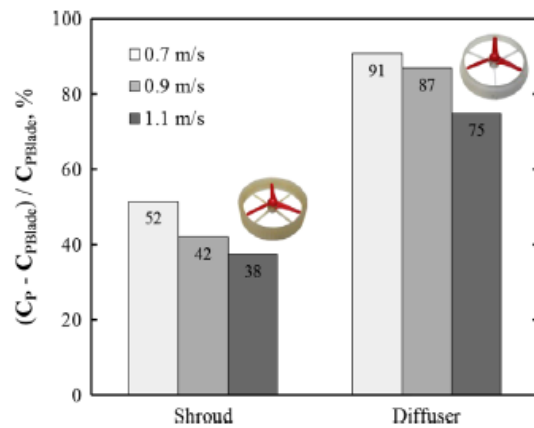
**Figure 2. 3** Relative increase in the maximum power coefficients
of the shrouded turbine over the bare turbine[40]

Shahsavarifard et al. performed experimental work and design a diffuser for the hydro-kinetic floating turbine. Four different diffusers geometries were design having different outlet area ratio. The speed of the incoming flow was varying from$1ms^{-1}$ to$3ms^{-1}$. The comparison of

output-power for both bare turbine and diffuser augmented hydro-kinetic floating turbine confirmed the advantage of using a diffuser[41].

Jo et al. investigated the effect of inclined angle, shapes of inlet and outlet and volume of the diffuser on its velocity amplification performance. Different geometries were considered for this purpose. In case 1 the diffuser angle was varied, whereas in case 2 a curved outer surface was considered to avoid the flow separation near the inlet area. The case 3 considered the combined effect of inclined angle and curved interior surface. In addition, both cases 2 and 3 had the special outlet shapes for the formation of negative pressure due to suction effects (as shown in Figure 2.4).
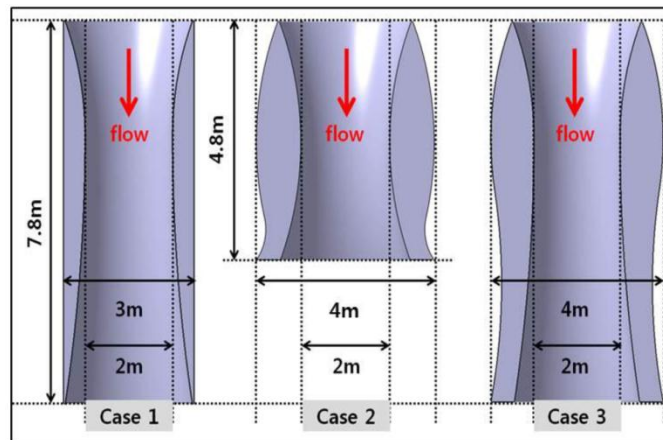
Figure 2. 4 3-D duct design[42]

A series of the numerical simulation were performed using commercial computational fluid dynamics (CFD) code ANSYS-CFX. The numerical results were validated against the experimental investigations conducted using a circulation water channel (CWC). A significant amplification in flow velocities was observed in all cases. In case 2 and 3, huge vortices were observed near the outlet area. Negative pressures near the outlet area in Case 2 and Case 3 contributed towards the duct performance due the suction effects [42].

Elbatran et al. proposed a prototype of a diffuser augmented horizontal axis marine current turbine to harness the energy from the low speed Malaysian ocean currents. A marine turbine with a rotor diameter of 0.66m was designed using NACA 0014 profile. The effenciecy of the turbine system was evaluated experimentally at Marine Technology Center (MTC), Malaysia.

The output power of the diffuser augmented turbine increased from 166 W (in case of bare turbine) to around 249 W [43].

Ganden and Bibeau coupled an analytical model with a Reynolds averaged Navier–Stokes (RANS) based computational fluid dynamics (CFD) solver to evaluate the ducted turbine designs. The comparison of the ducted and bare turbine results confirmed the increase in the power extracted by a turbine. Moreover, a significant reduction in the duct's mass flow efficiency was observed due to loading (as shown in figure 2.5), showing that the system will be more efficient when lightly loaded [44].
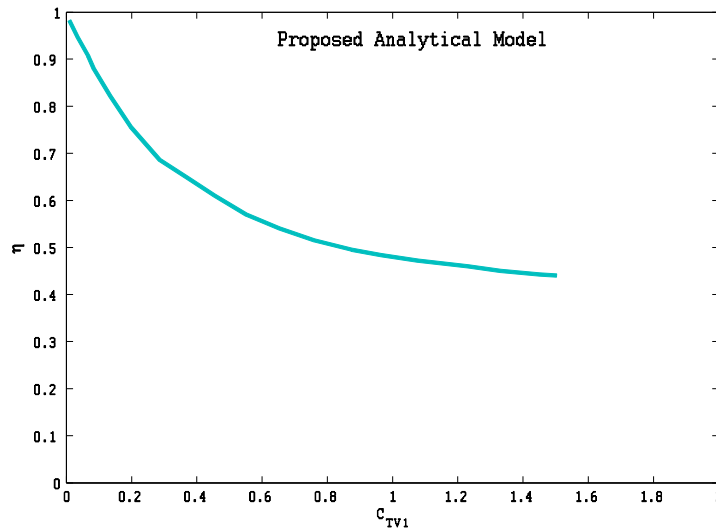
Figure 2. 5 η as a function of loading[44]

2.2 Missing Links in Literature

The work done on diffuser augmented HAHT so far shows that the advantages of using a diffuser around the HAHT are recognized. There is an increasing trend/ focus on designing HAHT with diffusers. In this context, a number of NACA airfoils have been implemented/ investigated. The diffuser augmented HAHT has only been around for a little over a decade, so it is expected that the research work so far is still in establishing stage and mature approaches for diffuser design are under research, conceptualization or yet to come.

The missing part or next step is the realization that most of the diffuser design for HAHT applications so far, has been based on standard NACA airfoils. Although this work has generated promising results, i.e. significant increase in power output. These airfoils are designed for high flow speed applications. Since the marine current velocity, most parts of the world, is almost 1 m/sec on average. The diffuser based on low flow speed hydrofoil will be ideal for HAHT applications

CHAPTER 3

Mathematical Modeling

The performance of the diffuser augmented hydro kinetic turbines has conventionally been evaluated using three different techniques i.e. experimental testing, simplified empirical formulation and numerical modeling [44-50]. Similarly, for numerical simulations, various approaches have been used for rotor modeling ranging from a simple actuator disk model to full rotor representation. However, the moving from simple to detailed modeling techniques also increases the associated computational cost [51-63].

For the current research, numerical simulation, solving the Reynolds-averaged Navier-Stokes equations, was selected as the method of choice. One of the main advantages of this method is the detailed flow field data which gives insight into the hydrodynamic performance of ducted turbines. This chapter provides a brief overview of the mathematical model used for the design and optimization of diffuser and to analyze the performance of the diffuser augmented hydrokinetic turbines.

3.1. Computational Fluid Dynamics and RANS Modeling

In fluid dynamics, the equations governing the motion and properties of the fluid flow are the mathematical form of basic conservation laws for mass, momentum and energy. The momentum equations for viscous flow are also known as "Navier-Stokes equations". The several alternative derivations of these equations can be found in the literature [57].

- Mass conservation ⟹ Continuity Equation
- Momentum conservation ⟹ Momentum Equation
- Energy conservation ⟹ Energy Equations

The present study does not involve heat equation due to the negligible heat transfer and incompressible flow conditions. The governing equations for two-dimensional, incompressible, steady state flow are as follows

$$\frac{\partial u_i}{\partial x_i} = 0 \tag{3.1}$$

$$\frac{\partial(\rho u_i u_j)}{\partial x_j} = -\frac{\partial p}{\partial x_i} + \frac{\partial \tau_{ij}}{\partial x_j} \tag{3.2}$$

$$\tau_{ij} = \left[\mu\left(\frac{\partial u_i}{\partial x_j} + \frac{\partial u_j}{\partial x_i}\right)\right] - \frac{2}{3}\mu\frac{\partial u_i}{\partial x_j}\delta_{ij}$$

Here x_i, u_i ρ, p and τ_{ij} are the ith, j^{th} spatial dimension, i^{th}, j^{th} component of velocity, density, pressure and Reynolds Stress respectively.

3.1.1 Reynolds-averaged Navier-Stokes equations

Generally the fluid flow is divided into two broad categories, laminar and turbulent flow. In case of laminar flow, the fluid flow in parallel layers and has a very small property transfer between the adjacent layers. On the other hand, turbulent flows are characterized by three-dimensional, very irregular, random and highly rotational flows. Whether a flow is laminar or turbulent depends on the Reynolds number which is a ratio of inertial to viscous forces, i.e.

$$Re = \frac{\rho u L}{\mu} \tag{3.3}$$

Here L is the flow characteristic length scale. Laminar flows occur at low Reynolds numbers where the viscous forces are dominant. Similarly turbulent flows arise at high Reynolds numbers and are dominated by inertial forces.

As mentioned by Gerber et al. the flow around a typical tidal turbine should always be simulated under the realistic turbulent tidal flow conditions. Thus, the flow equations are required to be solved for a turbulent flow field [58]. Direct numerical simulation (DNS) is one option to cater such problems, which solves Navier–Stokes equations numerically using a very fine mesh. Thus, it solves all of the relevant spatial and temporal scales of the turbulent flow field without any turbulence model. So DNS are computationally very expensive and is most suitable for simple geometries [59].

The Reynolds-averaged Navier-Stokes (RANS) equations are comparatively inexpensive and most commonly used approach to model turbulent flows. The Navier-Stokes equations are transformed into the RANS equations by decomposing instantaneous quantities into their time-averaged and fluctuating parts. This process decomposition of a flow variable is also known as

Reynolds decomposition. The Reynolds decomposition of the velocity components u_i, v_i and pressure p is:

$$u_i = \overline{u_i} + \acute{u}_i \tag{3.4}$$

$$v_i = \overline{v_i} + \acute{v}_i \tag{3.5}$$

$$p = \bar{p} + \acute{p} \tag{3.6}$$

The above method has considered the mean of the fix point in space and averaged it over time span that is large enough for mean value to be independent of it.

$$\bar{u} = \frac{1}{\nabla t} \int_{t_o}^{t_o+t_1} u \, dt \tag{3.7}$$

Time averaged of perturbing variable are set to zero.

$$\bar{\acute{u}} = \bar{\acute{v}} = \bar{\acute{p}} = 0 \tag{3.8}$$

Substituting the mean and fluctuating components of velocity in the continuity equation

$$\frac{\partial \bar{u}}{\partial x} + \frac{\partial \acute{u}}{\partial x} + \frac{\partial \bar{v}}{\partial y} + \frac{\partial \acute{v}}{\partial y} = 0 \tag{3.9}$$

Time averaging the above equation

$$\overline{\frac{\partial \bar{u}}{\partial x} + \frac{\partial \acute{u}}{\partial x} + \frac{\partial \bar{v}}{\partial y} + \frac{\partial \acute{v}}{\partial y}} = 0 \tag{3.10}$$

Before moving forward, a few rules for time averaging are given below

$$\overline{\frac{\partial \bar{u}}{\partial x}} = \frac{1}{\nabla t} \int_{t_o}^{t_o+t_1} \frac{\partial u}{\partial x} dt = \frac{\partial}{\partial x} \frac{1}{\nabla t} \int_{t_o}^{t_o+t_1} u \, dt = \frac{\partial \bar{u}}{\partial x} \tag{3.11}$$

$$\overline{\frac{\partial \acute{u}}{\partial x}} = \frac{1}{\nabla t} \int_{t_o}^{t_o+t_1} \frac{\partial \acute{u}}{\partial x} dt = \frac{\partial}{\partial x} \frac{1}{\nabla t} \int_{t_o}^{t_o+\nabla t} \acute{u} dt = 0 \tag{3.12}$$

$$\bar{\bar{u}} = \bar{u}; \quad \overline{u+v} = \bar{u} + \bar{v}; \quad \overline{\bar{u}.u} = \bar{u}.\bar{v} \tag{3.13}$$

$$\overline{\int f ds} = \int \bar{f} \, ds; \overline{f \cdot g} \neq \bar{f} \cdot \bar{g}$$

Since the averaged derivatives of the fluctuationing part of a variable is zero, so that the time averaged continuity equation becomes

$$\frac{\partial \bar{u}}{\partial x} + \frac{\partial \bar{v}}{\partial y} = 0 \tag{3.14}$$

Similarly substituting the flow variables in x component of momentum equation in terms of mean and fluctuating components and apply time averaging

$$\rho\overline{\left[\left[\frac{\partial\overline{(\bar{u}+\acute{u})^2}}{\partial x} + \frac{\partial(\bar{u}+\acute{u})(\bar{v}+\acute{v})}{\partial y}\right] = \frac{\partial(\bar{p}+\acute{p})}{\partial x} + \mu[\frac{\partial^2(\bar{u}+\acute{u})}{\partial x^2} + \frac{\partial^2(\bar{u}+\acute{u})}{\partial y^2}\right]} \tag{3.15}$$

From references

$$\rho[\frac{\partial\overline{(u)}}{\partial t} + \frac{\partial\overline{(uu)}}{\partial x} + \frac{\partial\overline{(uv)}}{\partial y} + \frac{\partial\overline{(\acute{u}\acute{u})}}{\partial x} + \frac{\partial(\acute{u}\acute{v})}{\partial x} = F_x - \frac{\partial(\bar{p})}{\partial x} + \mu\left[\frac{\partial^2(\bar{u})}{\partial x^2} + \frac{\partial^2(\bar{u})}{\partial y^2}\right] \tag{3.16}$$

Naiver stoke equation for x-component

$$\rho\left[\frac{\partial(\bar{u})}{\partial t} + \bar{u}\frac{\partial(\bar{u})}{\partial x} + \bar{v}\frac{\partial\bar{u}}{\partial y}\right] = F_x - \frac{\partial(\bar{p})}{\partial x} + \mu\left[\frac{\partial^2(\bar{u})}{\partial x^2} + \frac{\partial^2(\bar{u})}{\partial y^2}\right] - \rho\left[\frac{\partial\overline{(\acute{u}\acute{u})}}{\partial x} + \frac{\partial\overline{(\acute{u}\acute{v})}}{\partial y}\right] \tag{3.17}$$

For Y-component

$$\rho\left[\frac{\partial(\bar{u})}{\partial t} + \bar{u}\frac{\partial(\bar{v})}{\partial x} + \bar{v}\frac{\partial\bar{v}}{\partial y}\right] = F_x - \frac{\partial(\bar{p})}{\partial y} + \mu\left[\frac{\partial^2(\bar{v})}{\partial x^2} + \frac{\partial^2(\bar{v})}{\partial y^2}\right] - \rho\left[\frac{\partial\overline{(\acute{u}\acute{v})}}{\partial x} + \frac{\partial\overline{(\acute{v}\acute{v})}}{\partial y}\right] \tag{3.18}$$

The general form of Reynolds-Averaged Naiver-Stokes (RANS) equation

$$\frac{\partial(\rho u_i)}{\partial t} + \frac{\partial(\rho u_i u_j)}{\partial x_j} = -\frac{\partial p}{\partial x_i} + \frac{\partial \tau_{ij}}{\partial x_j} + \frac{\partial(-\rho\overline{\acute{u}_i\acute{u}_j})}{\partial x_j} \tag{3.19}$$

Where $(u_j)'$ is the Instantaneous velocity component $(j = 1,2)$

In above equation, the additional shear stress terms $-\rho\overline{\acute{u}_i\acute{u}_j}$ due to turbulent mixing, is called Reynolds stresses. The addition of this new term requires one more equation for Reynolds stress tensor. A turbulence model can provide closure to the RANS equations and offers a solution for the Reynolds stresses.

The different turbulence model developed so far can be broadly divided in two categories, i.e. Reynolds stress models and eddy viscosity models. In Reynolds stress models, the stresses are modeled directly through a set of six transport equations (one for each stress), thus requires the solution of six additional transport equations. Since all stresses are computed directly, these models do not require isotropy in the stresses. However, the additional complexity makes these models expensive to solve, and they are therefore not widely used. On the other hand, only one or two additional transport equations are required in eddy viscosity models.

All the eddy viscosity models use the Boussinesq hypothesis to relate the Reynolds stresses to the mean velocity gradients.

$$-\rho\overline{\acute{u}_i\acute{u}_j} = -\frac{2}{3}\rho k\delta_{ij} + \mu_t\left(\frac{\partial u_i}{\partial x_j} - \frac{\partial u_j}{\partial x_i}\right) \tag{3.20}$$

where μ_t is the turbulent viscosity and k is the turbulent kinetic energy.

Depending on the number of additional equations solved to compute the turbulent viscosity coefficient μ_t, the eddy-viscosity models can be divided in three main categories [60].

1. Algebraic models
2. One equation models
3. Two equation models

Unfortunately there is no single turbulence model accepted universally for all classes of problems. So the choice of a suitable turbulence model depends on the various factors i.e. flow physics, the established practices for a specific application etc. The Spalart–Allmaras's model is considered as a most suitable choice in aerospace applications for simulating the wall bounded flows with adverse pressure gradients. The one-equation low-cost model solves a transport equation for the turbulent (eddy) viscosity and is given by [61]

$$\rho U_j \frac{\partial \tilde{v}}{\partial x_j} = c_{b1}\tilde{S}\tilde{v} + \frac{1}{\sigma}\frac{\partial}{\partial x_k}\left[(v + \tilde{v})\frac{\partial \tilde{v}}{\partial x_k}\right] + \frac{c_{b2}}{\sigma}\frac{\partial \tilde{v}}{\partial x_k}\frac{\partial \tilde{v}}{\partial x_k} - c_{w1}f_w\left[\frac{\tilde{v}}{d}\right]^2 \qquad (3.21)$$

Where

$$c_{b1} = 0.1355, c_{b2} = 0.622, c_{v1} = 7.1, \sigma = 2/3$$

$$c_{w1} = \frac{c_{b1}}{\kappa^2} + \frac{(1 + c_{b2})}{\sigma} , c_{w2} = 0.3, c_{w3} = 2, \kappa = 0.41$$

$$\chi = \frac{\tilde{v}}{v}, f_{v1} = \frac{\chi^3}{\chi^3 + c_{v1}^3}, f_{v2} = \frac{\tilde{v}}{1 + \chi f_{v1}}, f_w = g\left[\frac{1 + c_{w3}^6}{g^6 + c_{w3}^6}\right]^{1/6}, g = r + c_{w2}(r^6 - r)$$

$$r = \frac{\chi}{\tilde{S}\kappa^2 d^2}, \tilde{S} = S + \frac{\tilde{v}}{\kappa^2 d^2}, S = \sqrt{2\Omega_{ij}\Omega_{ij}}$$

Here v is the molecular viscosity, d is the distance from the wall and $\Omega_{ij} = \frac{1}{2}\left(\frac{\partial U_i}{\partial x_j} - \frac{\partial U_j}{\partial x_i}\right)$ is the rotation tensor.

3.2. Actuator Disc Modeling

In actuator disc approach, turbine inside a stream tube is replaced by a disc, with inlet and outlet boundaries at the far upstream and downstream of the disc (schematic shown in Figure 3.1). The flow passing through the disk is assumed to be steady, inviscid, incompressible and irrotational. Moreover, the pressure at the far upstream and downstream of the disc is equal to ambient static pressure. As the fluid passes through the disc, a discontinuous change in total pressure is created which results in fluid acceleration in downstream direction [62].
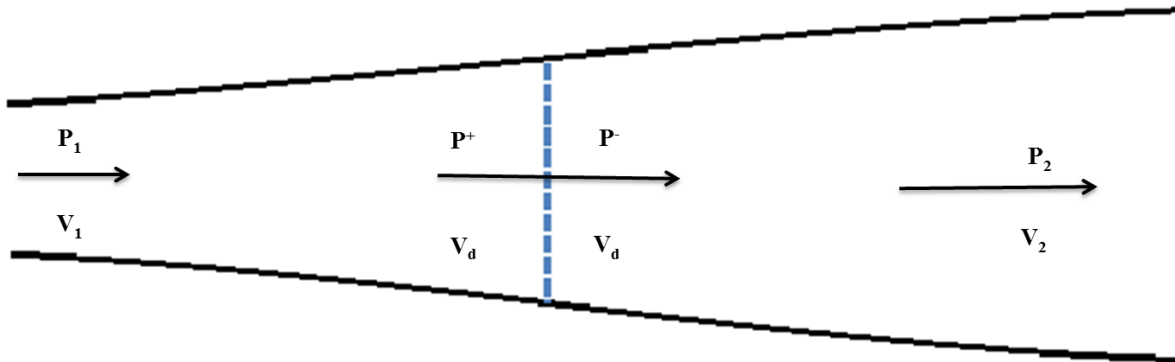

Figure 3. 1 Actuator disc model

Here P_1 is Static pressure, V_1 is the free steam velocity and A_1 is the area at the up steam of the actuator disk while P^+, V_d and A_d are pressure, velocity and area at the front of the actuator disk. Similarly P^-, V_d and A_d are the parameters at the back of actuator disk. The parameters at the downstream of the actuator are $P_1 V_3$ and A_2.

According to the equation of continuity

$$A_1 V_1 = A_2 V_2 = \text{constant} \tag{3.22}$$

According to the Bernoulli equation

$$P_1 + \frac{1}{2}\rho V_1{}^2 = P^+ \frac{1}{2}\rho V_d{}^2 \tag{3.23}$$

$$P^- + \frac{1}{2}\rho V_d{}^2 = P_1 + \frac{1}{2}\rho V_3{}^2 \tag{3.24}$$

Since the thrust force is directly proportionally to the pressure difference across the actuator disc, we can also represent thrust force in term of pressure drop.

$$T = \nabla P A_d \tag{3.25}$$

Where ∇P is pressure difference across the actuator disk and A_d is the area of the actuator disk. The pressure differences across the disc can also be found by

$$\nabla P = \frac{1}{2}\rho\left[V_1{}^2 - V_2{}^2\right] \tag{3.26}$$

Where ρ the density of the fluid, V_1 is is the free steam velocity of the flow and V_2 is the downstream velocity.

So, we can express the thrust force in term of pressure drop

$$T = \frac{1}{2}\rho A_d\left[V_1{}^2 - V_2{}^2\right] \tag{3.27}$$

The velocity at the actuator disc V_d and upstream and downstream velocities are related by

$$V_d = \frac{1}{2}[V_1 + V_2] \tag{3.28}$$

The axial induction factor (a) measures of the effect of actuator disc on the free stream velocity and is given by

$$a = \frac{V_1 - V_d}{V_1} \qquad (3.29)$$

Where V_1 is the free steam velocity and V_d is velocity at actuator disc. From above equation

$$V_d = V_1[1 - a] \qquad (3.30)$$

The downstream velocity can also be expressed in terms of axial induction and free steam velocity.

$$V_2 = V_1[1 - 2a] \qquad (3.31)$$

Similarly, the total thrust force on actuator disc in term of the axial induction factor.is

$$T = 2\rho A_d V_1^2 a[1 - a] \qquad (3.32)$$

Now the thrust co-efficient is defined as.

$$C_T = \frac{T}{\left[\frac{1}{2}\rho A_d V_1^2\right]} \qquad (3.33)$$

and thrust co-efficient in term of axial induction is

$$C_T = 4a[1 - a] \qquad (3.34)$$

The power extracted by the actuator disc from the incoming flow is directly proportionally to the product of thrust and velocity at the actuator disc.

$$P = TV_d \qquad (3.35)$$

The power is directly proportionally to the cube root of incoming velocity or the free steam velocity i.e.

$$P = 2\rho A_d V_1^3 a[1 - a]^2 \qquad (3.36)$$

The power co-efficient is the ratio of two parameters i.e power extracted from the flow and power available in the flow.

$$C_P = \frac{P}{\frac{1}{2}\rho A_d V_1^3} \tag{3.37}$$

C_P can also be defined in term of axial induction factor.

$$C_P = 4a[1-a]^2 \tag{3.38}$$

To find the maximum thrust co-efficient C_T

$$\frac{dC_T}{da} = \frac{d}{da}[4a(1-a)] \tag{3.39}$$

$$= 4 - 8a \equiv 0$$

$$a = \frac{1}{2}$$

Using $a = 1/2$ the maximum thrust co-efficient is

$$C_{Tmax} = 1$$

The maximum power co-efficient can be calculated in a similar manner

$$\frac{dC_P}{da} = \frac{d}{da}[4a(1-a)^2] \tag{3.40}$$

$$= 1 - 4a + 3a^2$$

Maximum power co-efficient at $a = 1/3$ is

$$C_{Pmax} = \frac{4}{3}\left[1-\frac{1}{3}\right]^2 \tag{3.41}$$

$$C_{pmax} = \left[\frac{16}{27}\right]$$

$$C_{pmax} = 0.593$$

The maximum power co-efficient obtained from this approach is 0.593 and is often referred as Betz limit.

3.3. Blade Element Momentum Theory

Blade Element Momentum Theory (BEM) is widely used for the design and performance analysis of wind and tidal turbines. It is a combination of the classical blade element theory and Froude's momentum theory. The blade element theory analyzes forces on turbine blade and depend on incoming flow velocity and blade geometry. The momentum theory performs a control volume analysis of conversation of momentum. These two methods result in a series of equations that can be solved iteratively. Following are the main steps of BEM (Blade Element Momentum Theory) [63]

Define the input data

1) Free steam Velocity (V_1)
2) Density of the flow (ρ)
3) Radius of the rotor (R)
4) Rotational rate (Ω)
5) Number of Blades (B)
6) Radius of the blade *(r)*

Step 1

Divide the rotor blade into n segments and input the following geometric parameters for each section

1) Twist Angle (β)
2) Chord length (L)
3) Pitch Angle (γ)

Step 2

Initial vaues of axial (a) and tangential induction factor (a') are set to zero i.e.

$$a = 0$$

$$a' = 0$$

Step 3

The angle (ϕ) and angle of attack α are calculated using relations given below

$$\phi = tan^{-1}\left[\frac{V_1(1-a)}{\Omega R(1+a')}\right] \tag{3.42}$$

$$\alpha = [\phi - (\beta + \gamma)] \tag{3.43}$$

Where Ω is rotational speed and R is radius of rotor

Step 4

The lift and drag coefficients are calculated from the known values of α from the previous step using

$$C_L(\alpha) = 0.327 + 0.1059\alpha - 0.013\alpha^2 \tag{3.44}$$

$$C_D(\alpha) = 0.006458 - 0.000272\alpha + 0.000219\alpha^2 - 0.0000003\alpha^3 \tag{3.45}$$

Step 5

The coefficients of normal and tangential forces for the turbine blade are evaluated using

$$C_n = C_L cos\phi + C_D sin\phi \tag{3.46}$$

$$C_t = C_L sin\phi - C_D cos\phi \tag{3.47}$$

Step 6

The values of normal and tangential force coefficients calculated in pervious step are now used to evaluate axial and tangential induction factors

$$a = \frac{1}{\frac{4sin^2\phi}{\sigma_r C_n} + 1} \tag{3.48}$$

Where $\sigma_r = \frac{BL}{2\pi R}$

$$a' = \frac{1}{\frac{4sin\phi cos\phi}{\sigma_r C_t} - 1} \tag{3.49}$$

Step 7

The values of axial and tangential induction factors calculated in step 7 are compared to those of previously assumed values. If the difference between two values is less than a selected tolerance, then iterative process is stopped and converged values of axial and tangential induction factors are used to calculate differential thrust, torque and power in step 9. Otherwise the iterative process is repeated for the desired convergence.

Step 8

The differential thrust, torque and power are calculated from previously converged values of axial and tangential induction factors

$$dT = 2F\rho V_1{}^2 a(1-a)2\pi r dr \qquad (3.50)$$

$$dQ = 2Fa'(1-a)\rho V_1 \Omega r^2 \qquad (3.51)$$

$$dP = \Omega dQ \qquad (3.52)$$

Step 9

The total power P, total thrust T and torque Q are estimated as sum of the $dQ, dT\ and\ dP$ from each span wise segment. The iterative procedure used for solving the BEM equations is also presented the form of flow chart given below.
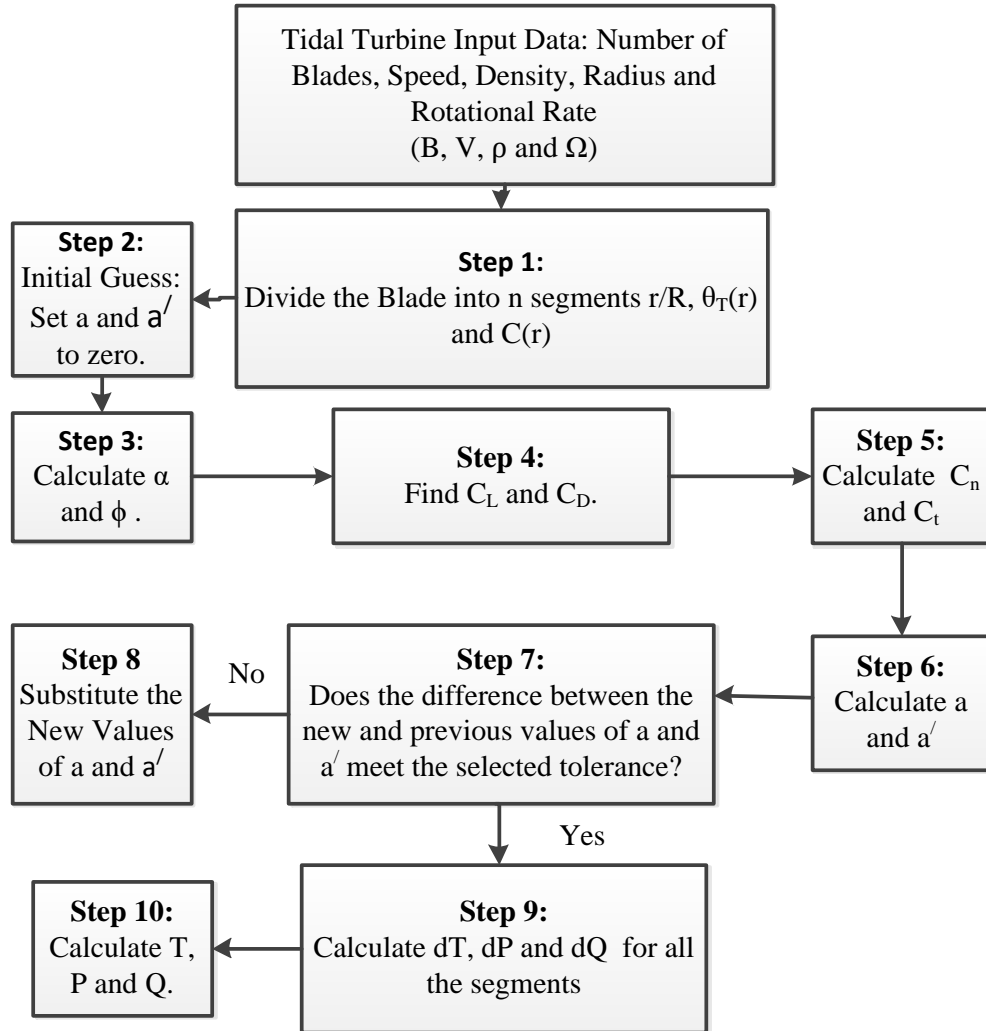
Figure 3. 2 Calculations flowchart of BEM theory

CHAPTER 4

Numerical Setup

The main focus of the current study is the design and optimization of a diffuser for hydrokinetic turbine application using computational fluid dynamic techniques. The reason for the selection of numerical simulation over the other available options (experimental testing and empirical formulations) is the significant reduction in requirement for resources, cost and time for such study.

The whole study is divided into three phases:

- Benchmark validation of flow over the flat plate airfoil
- Computational Analysis of performance of baseline diffuser generated from the flat plate airfoil. Diffuser optimization by achieving an optimum curved profile at the internal surface using computational techniques.
- performance analysis of optimized diffuser using numerical actuator disc approach

This chapter includes of details of the numerical setup used in current study.

4.1 Model Geometry

4.1.1 Case-1: Flat plate Airfoil

The flat plate airfoil is taken as a baseline geometry (shown in Figure below). The coordinates of the airfoil are listed in appendix A. The airfoil has a sharp trailing edge, a 5-to-1 elliptical leading edge, 1.96% thickness-to-chord ratio (shown in figure). Geometry and mesh generation software Gambit (version 2.4) is used to create the model geometry.
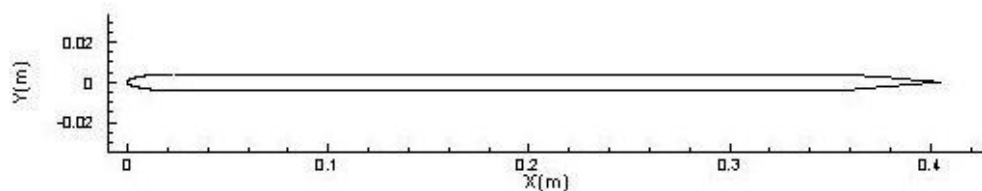
Figure 4. 1 Flat Plate airfoil geometry

4.1.2 Case-2: 2-D Diffuser

In the second phase of the study, the flat plate airfoil is used to design a baseline diffuser for horizontal axis hydrokinetic turbine application. Diffuser parameters are summarized in Table 4.1

Table 4. 1 Parameters of diffuser

Parameter	Value
Diffuser Length	0.380m
Inlet Diameter	0.500m
Incoming Flow Velocity	2.75m/s

## 4.2 Computational Domain and Mesh

4.2.1 Case-1: Flat plate Airfoil

The computational domain considered around the flat plate airfoil is of rectangle shape. The distance of the inlet and outlet boundaries from the flat plate airfoil leading and trailing edge, is 7c and 14c (c is the cord length of airfoil) respectively. Three systematically refining 2-D structured meshes are created by increasing the number of nodes on the surface of the airfoil. Mesh generation software Gambit is used for this purpose.

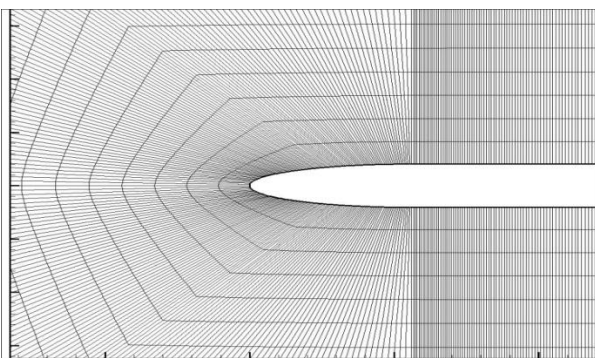**Table 4. 2** Parameters of mesh independence study

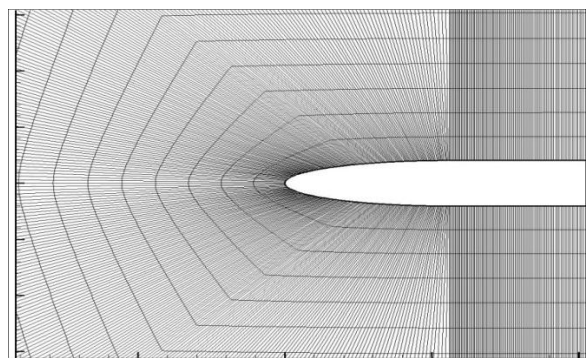| Mesh	Total no. of Cells	No. of Cells on Airfoil Surface
Coarse	24000	100
Medium	60000	200
Fine	114000	300
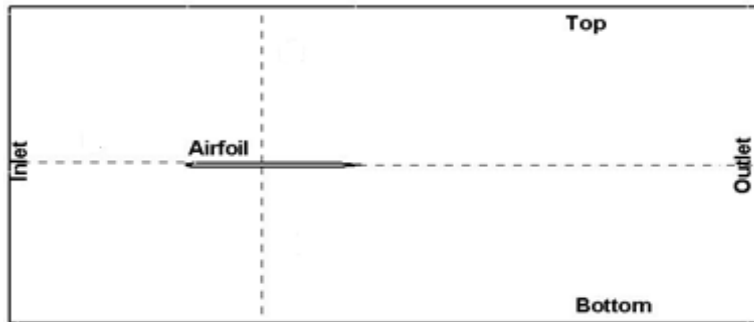
Figure 4. 2 Computational domain around flat plate airfoil
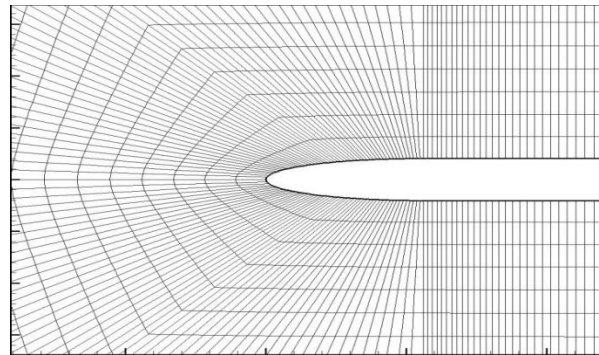
Figure 4. 3 Computational Mesh around flatplate airfoil leading edge: Coarse Mesh

Figure 4. 4 Computational Mesh around flat plate airfoil leading edge Medium Mesh

Figure 4. 5 Computational Mesh around flat plate airfoil leading edge Fine Mesh

In order to achieve a y^+ value in an acceptable range, the distance of the first node from the wall is calculated using below formula [64]

$$\Delta y = \frac{y^+ \mu}{U_\tau \rho} \tag{4.1}$$

Where

$$U_\tau = \sqrt{\frac{\tau_w}{\rho}} \tag{4.2}$$

$$\tau_w = \frac{1}{2} C_f \rho U_\infty{}^2 \tag{4.3}$$

$$C_f = 0.058 Re^{-0.2} \tag{4.4}$$

L is flow characteristic length scale and Re is the Reynolds Number. It can be observed that the y^+ is a function of local fluid velocity, which changes significantly across the airfoil surface. Hence, it is impossible to know exact the value y^+ before running an initial simulation. However, a reasonable early approximation of the first node distribution can be reached using this method.

4.2.1.1   Grid Independence Study

In order to perform grid convergence study, the Grid Convergence Index (GCI) is used to measure the relative discretization error in the simulated results. This method is based on the Richardson Extrapolation technique and is regarded as one of the most reliable methods for the measuring the grid convergence errors in the numerical solution of partial differential equations. As per Roaches recommendations, three mesh schemes are considered for assessment of discretization error via GCI using below procedure [65, 66]

Step 1: The representative grid size h is defined using

$$h = \left[\frac{1}{N} \sum_{i=1}^{N} (\Delta A_i) \right]^{1/2} \tag{4.5}$$

Where A is the area of the ith mesh elements and N is the total number of mesh points. The mesh refinement factor (r) is estimated using the formula given below

$$r = {h_{coarse}}\big/{h_{fine}} \qquad (4.6)$$

For a mesh refinement scheme with three successively increasing mesh schemes, grid refinement factor must be greater than 1.3.

Step 2: Let $h_1 < h_2 < h_3$ and $r_{21} = h_2/h_1$, $r_{32} = h_3/h_2$. The apparent order p is calculated using equations

$$p = \frac{1}{\ln{(r_{21})}} \left| \ln\left| {\mathcal{E}_{32}}\big/{\varepsilon_{21}} \right| + q(p) \right| \qquad (4.7)$$

$$q(p) = \ln\left(\frac{r_{21}^{p} - s}{r_{32}^{p} - s} \right) \qquad (4.8)$$

$$s = 1.\,sgn\left({\mathcal{E}_{32}}\big/{\varepsilon_{21}}\right) \qquad (4.9)$$

where $\varepsilon_{32} = \phi_3 - \phi_2, \varepsilon_{21} = \phi_2 - \phi_1$ and ϕ_k denotes the simulated result on the kth grid.

Step 3: The extrapolated solution is calculated using

$$\phi_{ext}^{21} = \frac{\left(r_{21}^{p}\phi_1 - \phi_2\right)}{\left(r_{21}^{p} - 1\right)} \qquad (4.10)$$

Step 4: Finally, the extrapolated relative error (e_{ext}^{21}) , approximate relative error (e_a^{21}) and GCI are given by

$$e_{ext}^{21} = \left| \frac{\phi_{ext}^{21} - \phi_1}{\phi_{ext}^{21}} \right| \qquad (4.11)$$

$$e_a^{21} = \left| \frac{\phi_1 - \phi_2}{\phi_1} \right| \qquad (4.12)$$

$$GCI_{fine}^{21} = \frac{1.25 e_a^{21}}{r_{21}^{p} - 1} \qquad (4.13)$$

4.2.2   Case-2: 2-D Diffuser

The computational domain in case of the diffuser is also rectangle type. The distance of the inlet and outlet boundaries from diffuser is 7L and 14L respectively (L is the length of diffuser). Similarly the distance of the top and bottom of the computational domain from diffuser is 1L and R (radius of the diffuser) respectively. The 2-D structured mesh scheme is used to mesh

computational domain. After performing the mesh independence study in case of flat plate airfoil, fine mesh (114000 cells) is used for all diffuser related computational (See details in chapter 5).
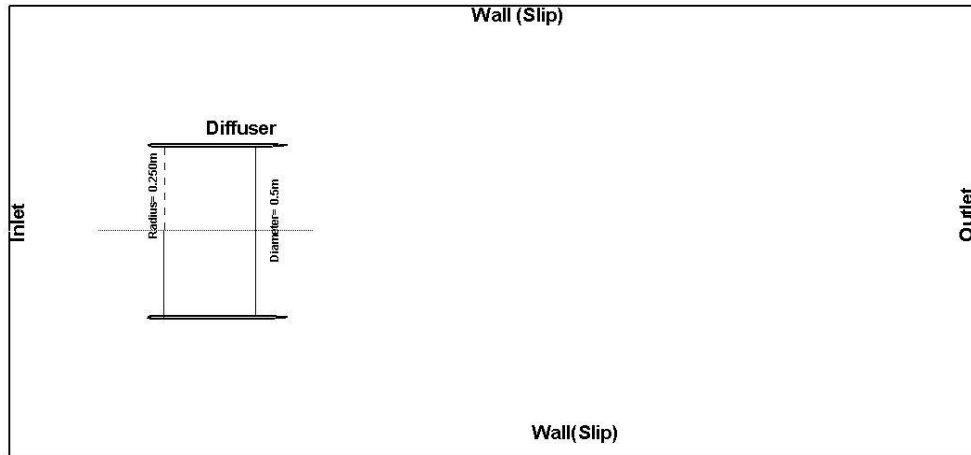
Figure 4. 6 Computational domain around diffuser

4.3 Boundary Conditions

4.3.1 Case-1: Flat plate Airfoil

The velocity of the incoming flow is $7.84 m/s$ (giving Re $= 1 \times 10^5$). Similarly the fluid density and viscosity are 1.77kgm^{-3} and $1.846 \times 10^{-5} \text{ m}^2/\text{s}$ respectively. The boundary conditions at inlet, outlet and other flow boundaries are summarized in Table 4.3.

Table 4. 3 Boundary conditions for flow past flat plate airfoil

Zone	Boundary Condition
Airfoil Surface	Wall (No-Slip Condition)
Inlet	Velocity Inlet
Outlet	Pressure Outlet
Domain Top	Wall (Slip Condition)
Domain Bottom	Wall (Slip condition)

4.3.2 Case-2: 2-D Diffuser

In order to simulate the flow around 2-D diffuser, the incoming flow velocity is considered as 2.75m/s (giving $Re = 6 \times 10^5$). The fluid density and viscosity are 1028kgm^{-3} and 1.6435×10^{-3} m^2/s respectively. Similarly, the total temperature and pressure are set to $278k$ and 101325pa respectively.

Table 4. 4 Boundary conditions for flow around 2-D diffuser

Zone	Boundary Condition
Diffuser Surface	Wall (No-Slip Condition)
Inlet	Velocity Inlet
Outlet	Pressure Outlet
Domain Top	Wall (Slip Condition)
Symmetry Plane	Symmetry

4.4 Solver Settings

The two dimensional, incompressible, steady state flow around both flat plate airfoil and diffuser is simulated using finite volume based commercial software Ansys Fluent (16). The academic license of this software is available at Research Center for Modeling and Simulation (RCMS), National University of Sciences and Technology (NUST), H-12 Islamabad. The numerical simulations are performed on RCMS super computer using 4 compute nodes (each node consisted of 8 processors), available at Supercomputing Research and Education Center (ScREC), RCMS, NUST.

The well-known SIMPLE algorithm is used for pressure velocity coupling in the current study. Second-order-upwind interpolation schemes have been used for convection terms as they provide an improved computational accuracy by reducing numerical diffusion error. The convergence of the left and drag coefficients along the residual history is monitored to examine the iterative convergence. The root mean square (RMS) residual value of 10^{-6} is selected as the stopping criteria.

# CHAPTER 5

Results and Discussion

A series of simulations are conducted for the design and optimization of diffuser geometry using following steps

1. First the flow around the two-dimensional airfoil is simulated and numerically computed values of drag and lift coefficients are validated with available results.
2. Later, CFD analyses are carried out for baseline diffuser generated from the flat plate airfoil. The performance of this diffuser was optimized by achieving an optimum curved profile at the internal surface of the diffuser. Bézier curves parameterization and design of experiment (DOE) techniques are used for this purpose. The Response Surface Methodology (RSM) is used as a tool for optimization.
3. Finally the performance of the optimized diffuser is analyzed using numerical actuator disc approach.

This chapter provides a discussion of the main findings from the research.

5.1. Benchmark Validation

First the flow over 2-D flat plate airfoil is simulated to validate meshing strategy, boundary conditions and solution methodologies. An extensive experimental/numerical data is available for 2-D flat plate airfoil and is used for the validation purposes [67-68]. Steady-state simulations are performed at free stream velocity of 7.84m/s (based on the Reynolds number of 100,000). The various angles of attack (ranging from 0°-8°) are considered. The comparison between the computed and available results of lift and drag coefficients at different angles of attack is shown in Figure 5.1 . It can be observed that the simulated results are in good agreement with available data.
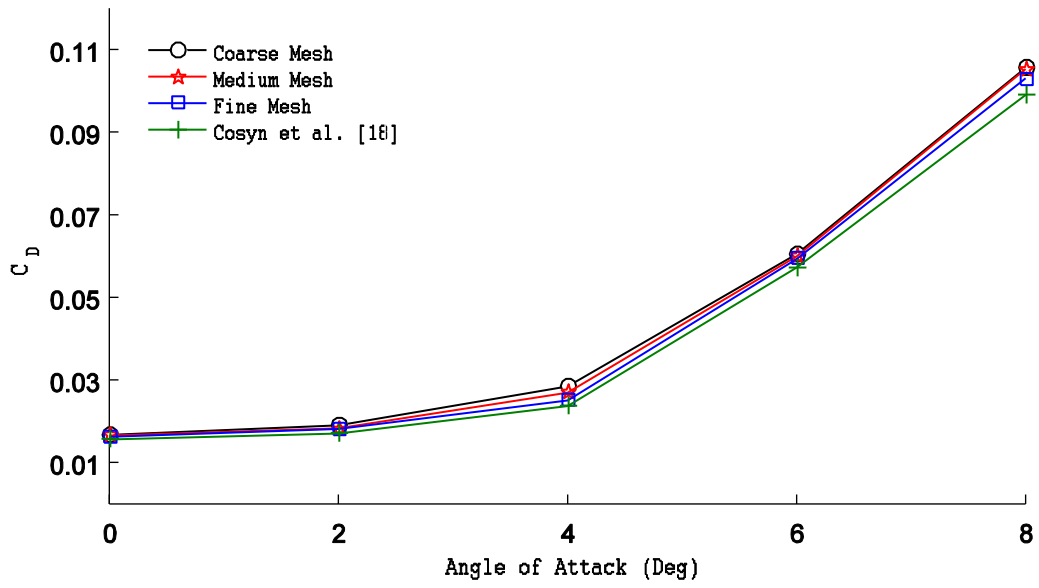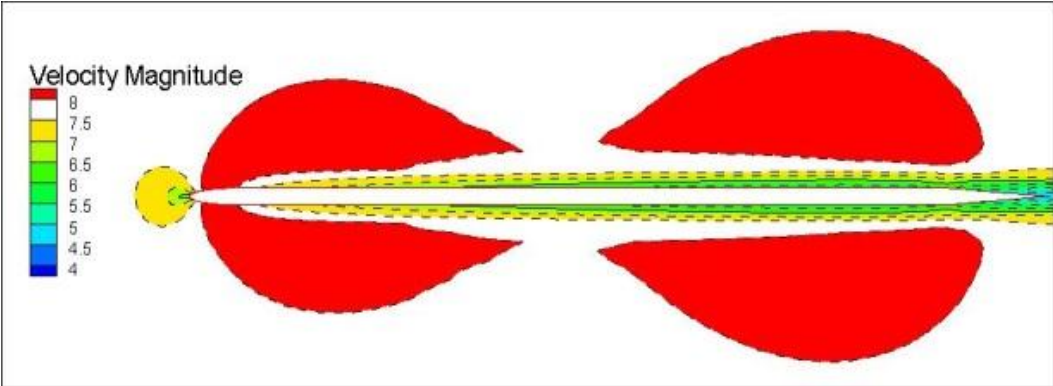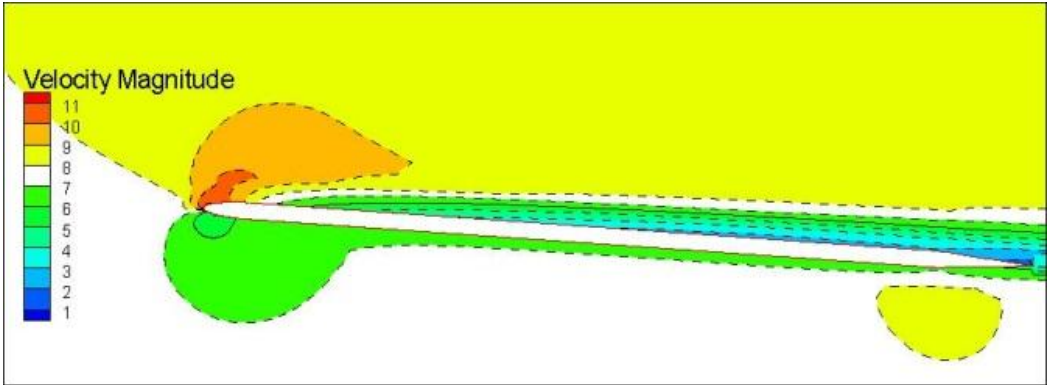
(a)

.
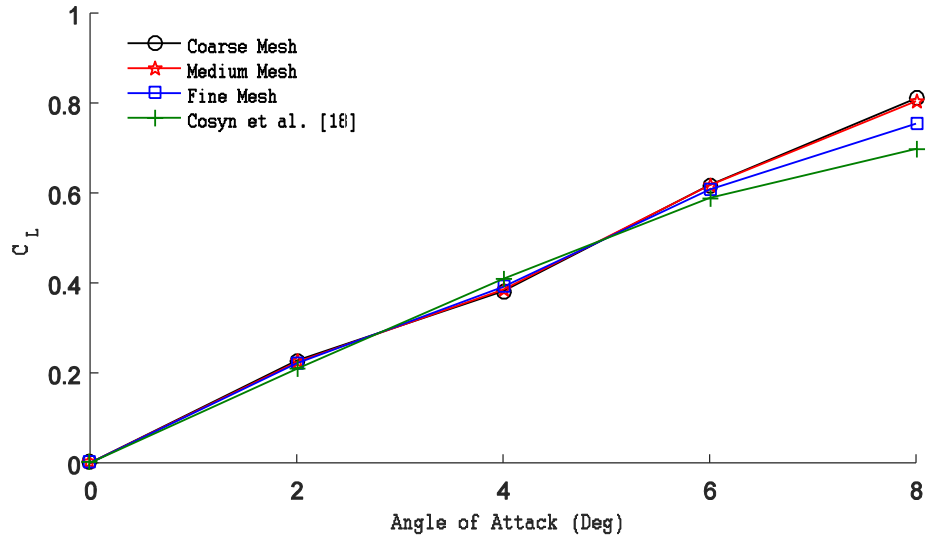
(b)

Figure 5. 1 Drag coefficient vs. angle of attack **(a)** Lift coefficient vs. angle of attack **(b)**
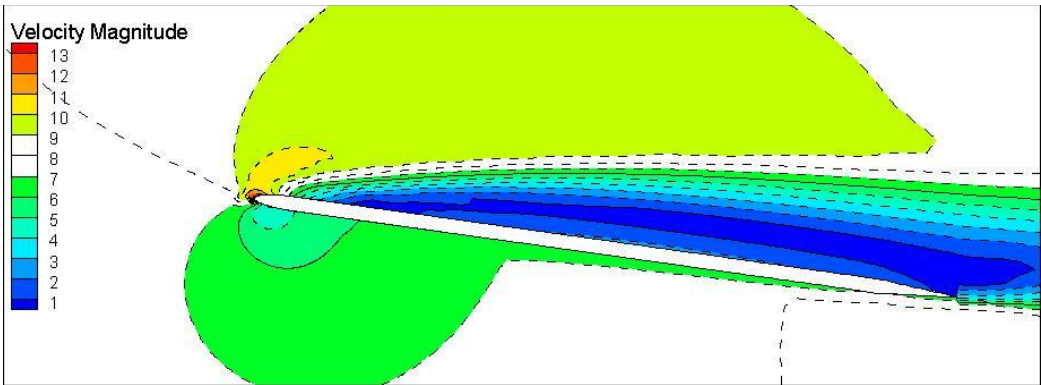
The velocity contours at three different angles of attack are shown in the Figure 5.2 At higher angle of attack, larger flow separation zone can be observed from these Figures.

(a)

(b)

(c)

Figure 5. 2 The contours of the Velocity Magnitude at different angle of attack : (a) Angle of attack 0^0;

b) Angle of attack 4^0 ; (c) Angle of attack 8^0.

5.1.1 Grid Convergence Study

The order of accuracy p and GCI for the two parameters, i.e. simulation results of lift and drag on three grids are summarized in the Tables 5.1 and 5.2 respectively. Superscripts 1, 2 and 3 represent coarse, medium and fine mesh respectively. It can be observed from Table 5.1 that GCI for finer grid (GCI^{32}) has relatively small value compared to that of the coarser grid (GCI^{21}) indicating a reduced dependency of numerical results on the cell size. Therefore, the further grid refinement would not offer a significant change in the numerical results. A similar behavior is observed for parameter of lift coefficient as well (see Table 5.2).

Since a negligible change in the solution is expected by the further mesh refinement, fine mesh (mesh 3) is used for all further computations.

Table 5. 1 Order of accuracy and grid convergence index for drag coefficient

Angle of Attack	e^{21}	e^{32}	p	GCI^{21}	GCI^{32}
0^0	2.01	1.21	0.31	16.27	16.25
2^0	3.48	1.09	1.57	4.13	2.63
4^0	4.64	2.02	0.97	10.28	4.68
6^0	1.76	0.43	1.97	1.94	1.49
8^0	3.69	3.31	0.54	16.46	9.10

Table 5. 2 Order of accuracy and grid convergence index for lift coefficient

Angle of Attack	e^{21}	e^{32}	p	GCI^{21}	GCI^{32}
0^0	7.755	6.463	0.286	69.181	17.908
2^0	2.495	0.675	1.827	2.381	2.160
4^0	2.250	0.594	1.826	3.529	2.162
6^0	3.471	0.894	1.935	3.041	2.001
8^0	2.786	0.728	1.895	2.519	2.059

5.2. Diffuser Design and Optimization

In the second phase of the study, a straight wall diffuser is designed using flat plate airfoil (parameters summarized in Table 4). Subsequently, the performance of the diffuser is optimized by achieving an optimum curved profile at the internal surface of the diffuser. The response surface based optimization approach is used for this purpose. The fluid velocity profile at the throat is considered as an objective function in this optimization study.

Table 5. 3 Parameters of diffuser

Parameter	Value
Diffuser Length	0.380m
Inlet Diameter	0.500m
Incoming Flow Velocity	2.75 m/s

The Response Surface based optimization procedure is carried out as follows:

1) Bezier curve parameterization technique is used to represent the airfoil.
2) In order to generate a response surface model, 3^k factorial design is used to determine the number of required numerical measurements of the response of interest.
3) The best-fitted surface to numerical data points is developed.
4) The optimal set of input parameters producing the optimum response value is determined.

5.2.1 Design of Experiments (DOE)

Airfoil shape parameterization is an important consideration in any airfoil optimization process. Over the past few decades, numerous parameterization techniques have been developed and being used. An extensive review of these shape parameterization techniques for airfoils can be found in [69]. Bezier parameterization is one of the most commonly used techniques to represent the shape of airfoil. The Bezier curve of order n+1 (degree n) requires n+1 control points and passes through the first and last control points (the initial and terminal point on the curve itself) [70].

In the present case, a 4th degree Bezier curve is used to fit symmetric flat plate airfoil. The first and last control points, P_0 and P_4 lie on the airfoil leading and trailing edges respectively. The position of P_0 is fixed. The remaining 4 control points are allowed to only move vertically (keeping the abscissas fixed). The following constraint was also set on the y coordinate of control points to obtain different conical diffusers and to maintain a realistic search space.

$$y_4 \geq y_3 \geq y_2 \geq y_1$$

A 3^k factorial design is used to determine the number of experiments required to create a response surface. Here k represents the number of varying parameters (y coordinates of 4 control points in the present case). Out of 81 different diffuser geometries, only 15 (shown in Figure 5.4) satisfied the above mentioned condition and are selected for further analysis.
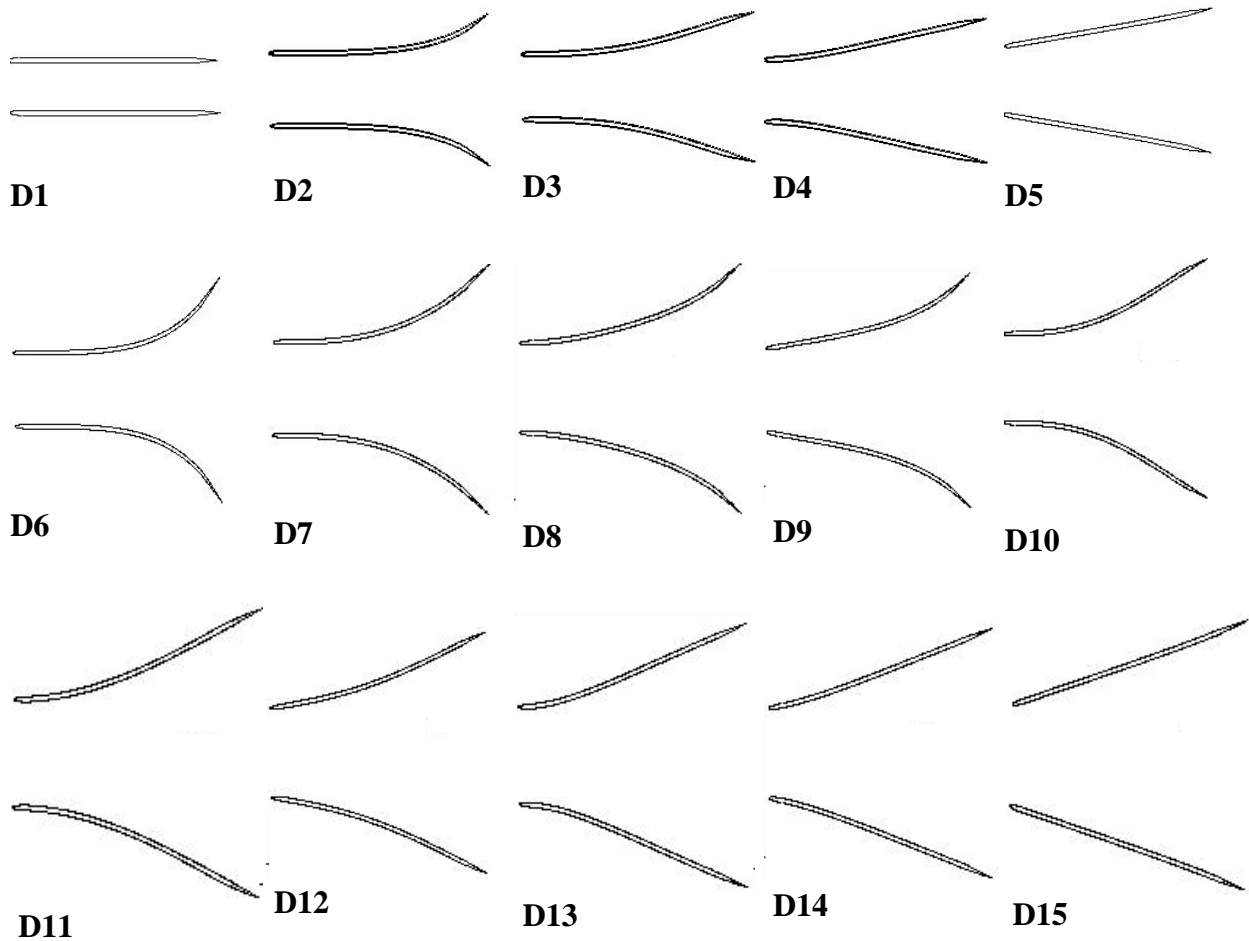
Figure 5. 3 Different diffuser configurations used for CFD analysis

The flow behaviour inside each diffuser is simulated using CFD techniques. The comparison of axial velocity distribution inside different diffusers is shown in Figure 5.4
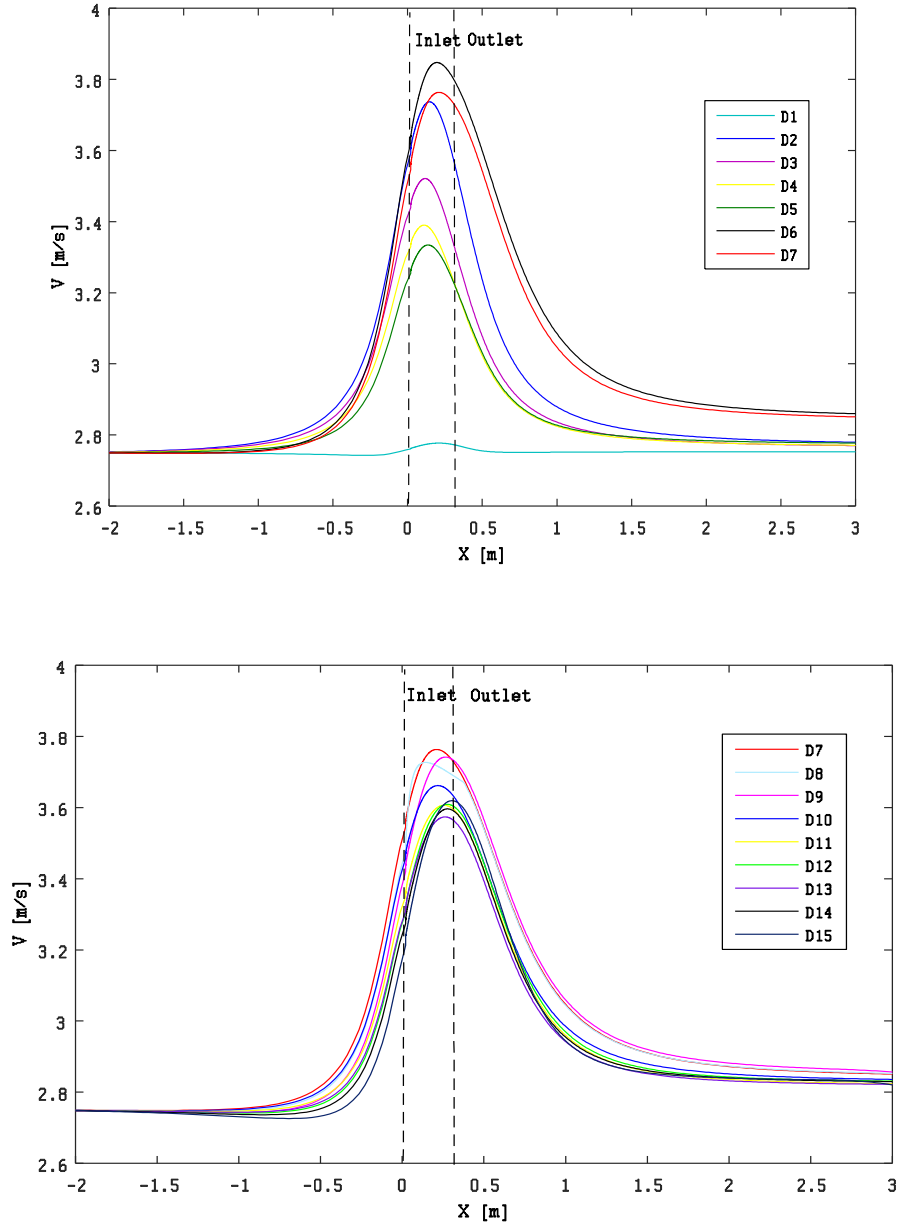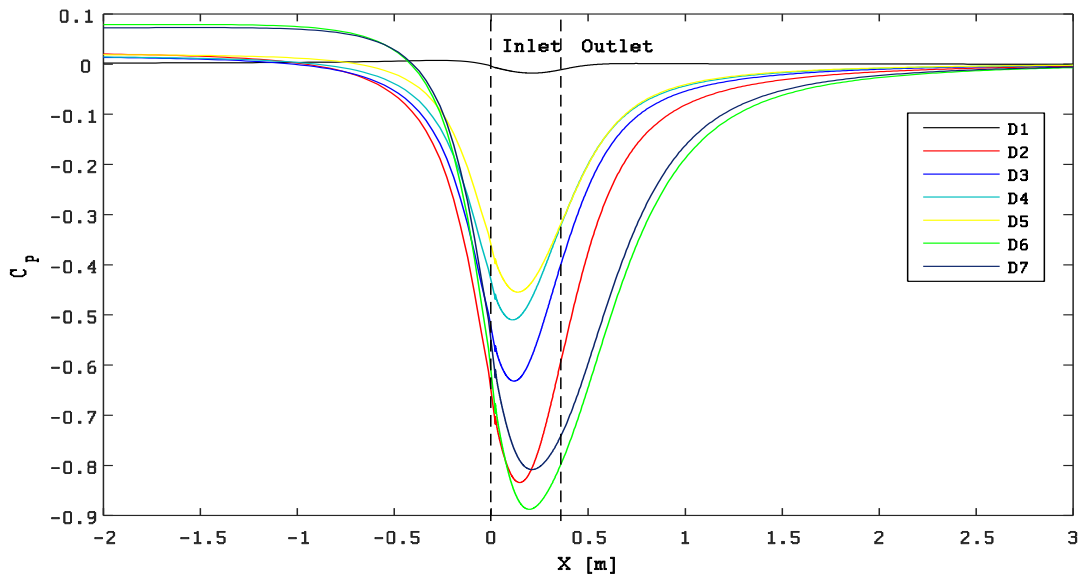

Figure 5. 4 Axial velocity distribution inside different diffusers

Similarly, Table 5.4 shows the value of the fluid velocity at throat of all investigated diffuser. It can be observed that diffuser D_6 produced the maximum velocity augmentation of 30.08% in comparison to the straight one (D_1).

Table 5. 4 Fluid Velocity at the diffuser throat

Diffuser Geometries	Velocity (m/s)	Diffuser Geometries	Velocity (m/s)
D_1	2.76	D_9	3.398
D_2	3.57	D_{10}	3.43
D_3	3.42	D_{11}	3.33
D_4	3.319	D_{12}	3.29
D_5	3.24	D_{13}	3.29
D_6	3.59	D_{14}	3.25
D_7	3.52	D_{15}	3.17
D_8	3.46		

The comparison of pressure distribution inside different diffusers is shown in Figure 5.5. Similarly Figure 5.6 shows the contours of velocity magnitude inside and around different diffusers.
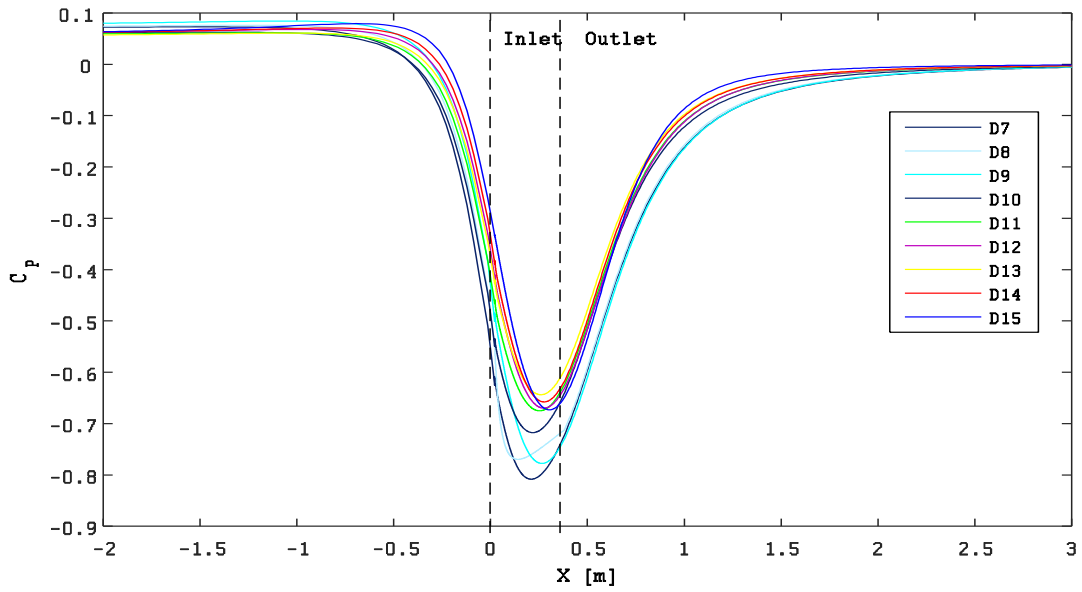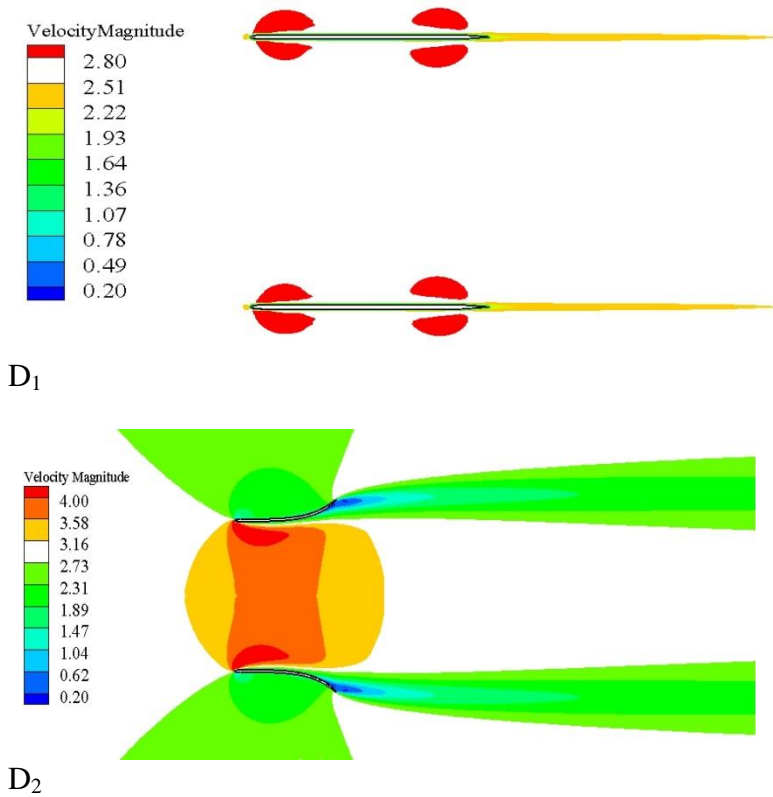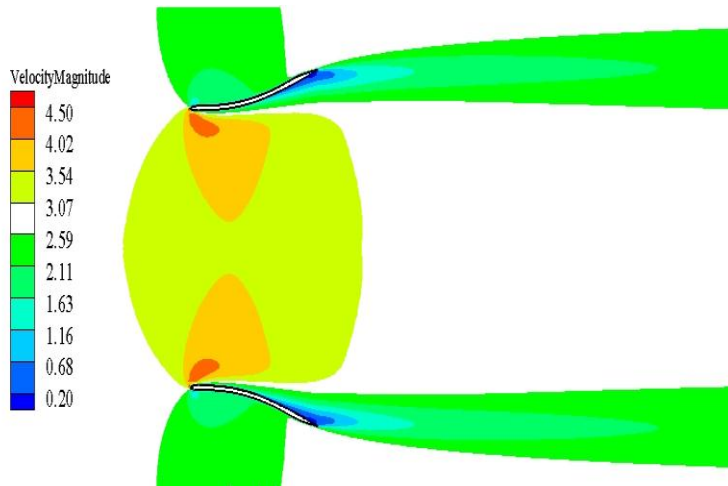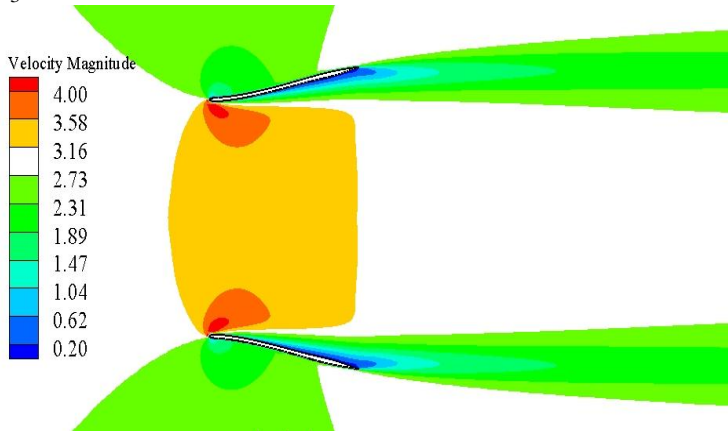
Figure 5. 5 Cp distribution in different diffuser

D₁

D₂

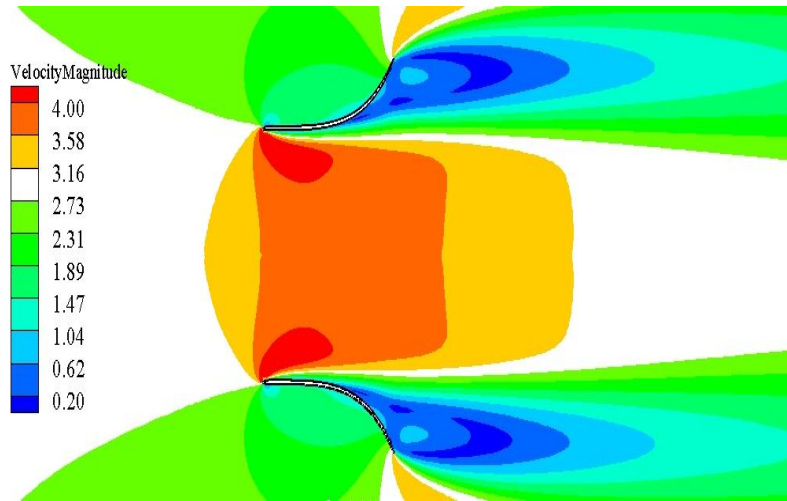VelocityMagnitude

4.50
4.02
3.54
3.07
2.59
2.11
1.63
1.16
0.68
0.20

D₃

Velocity Magnitude

4.00
3.58
3.16
2.73
2.31
1.89
1.47
1.04
0.62
0.20

D₄

Velocity Magnitude

4.00
3.58
3.16
2.73
2.31
1.89
1.47
1.04
0.62
0.20
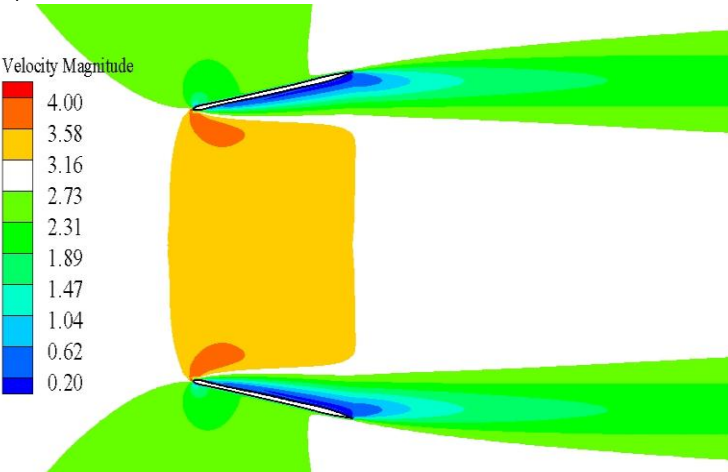
D₅

D_6
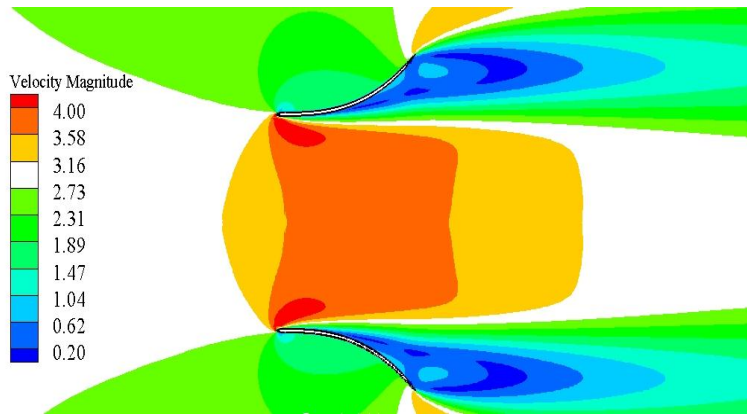
D_7
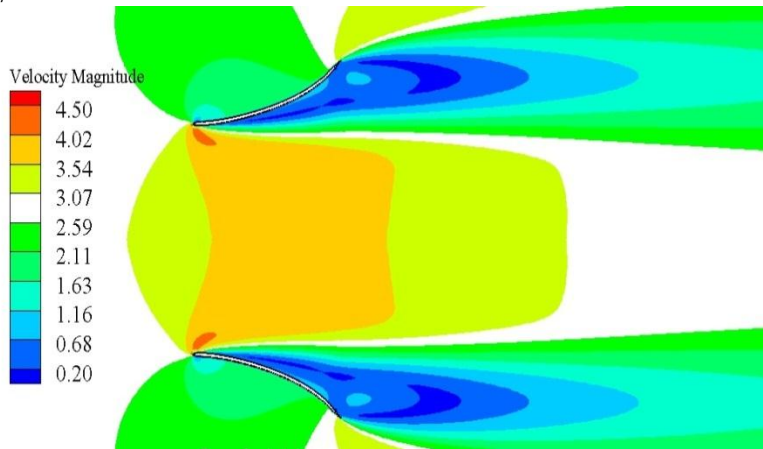
D_8
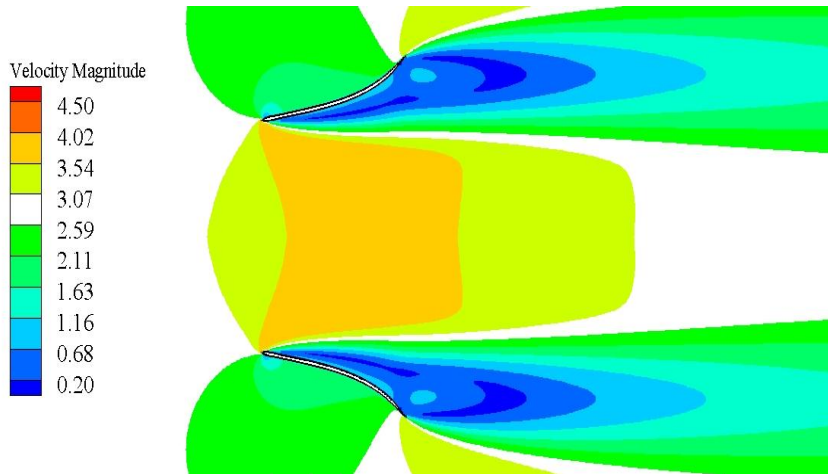
D$_9$

D$_{10}$

D$_{11}$

D$_{12}$

D$_{13}$

D$_{14}$

59
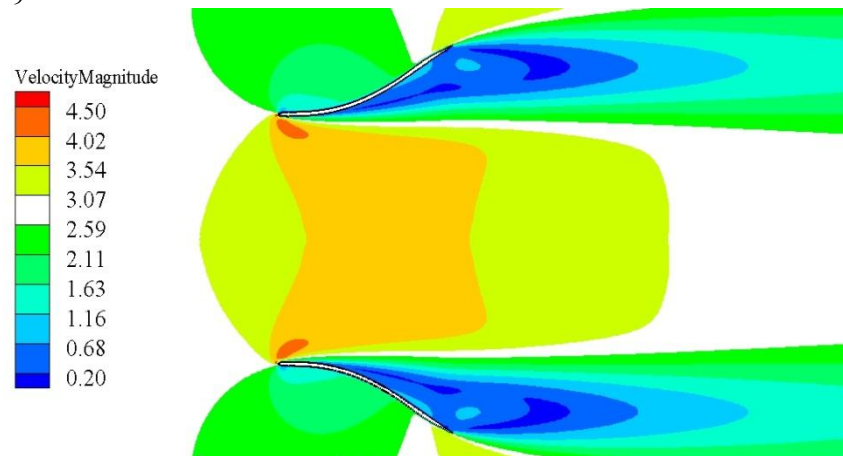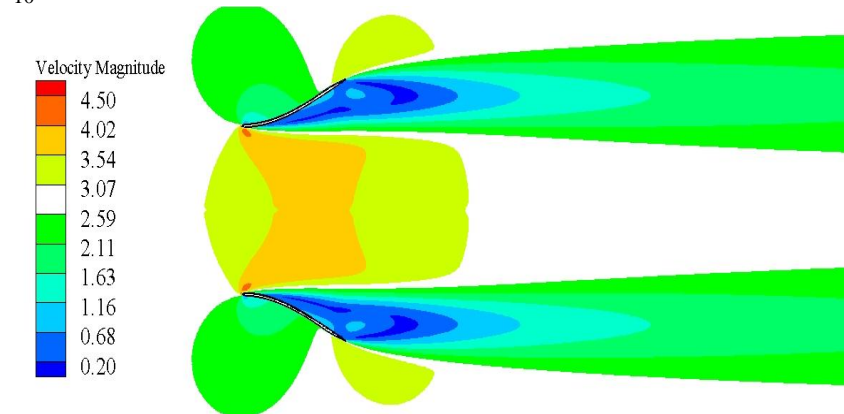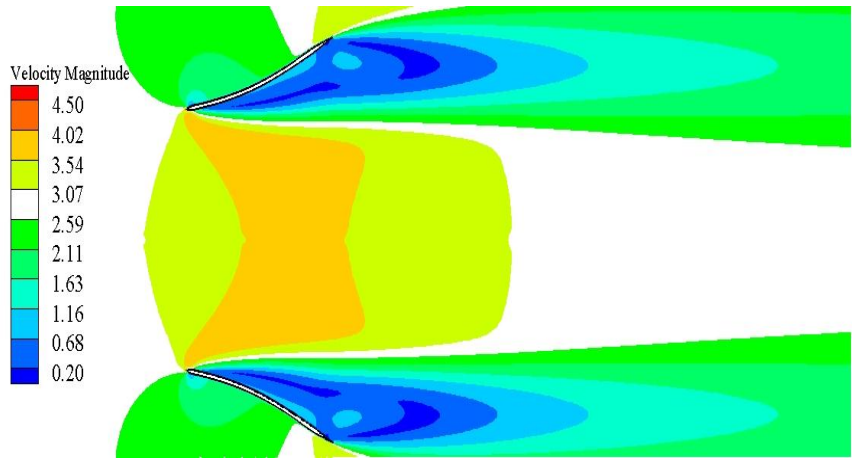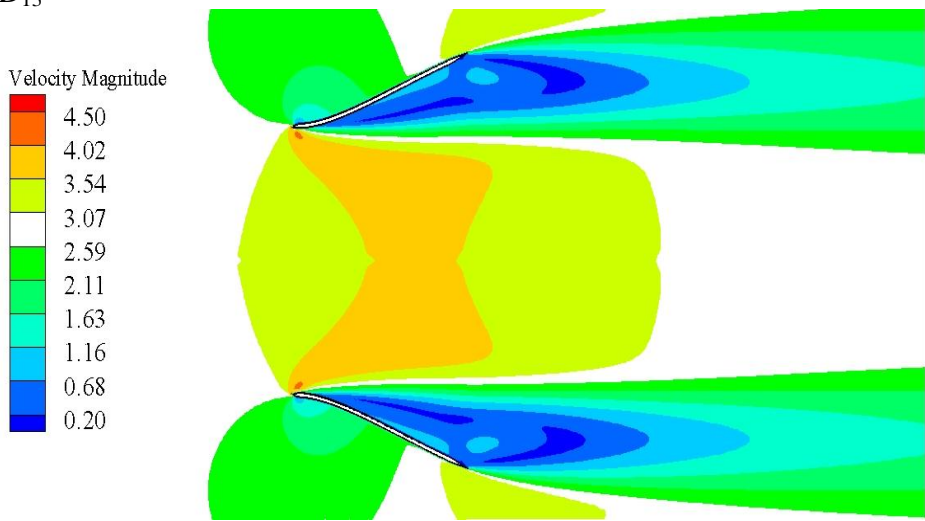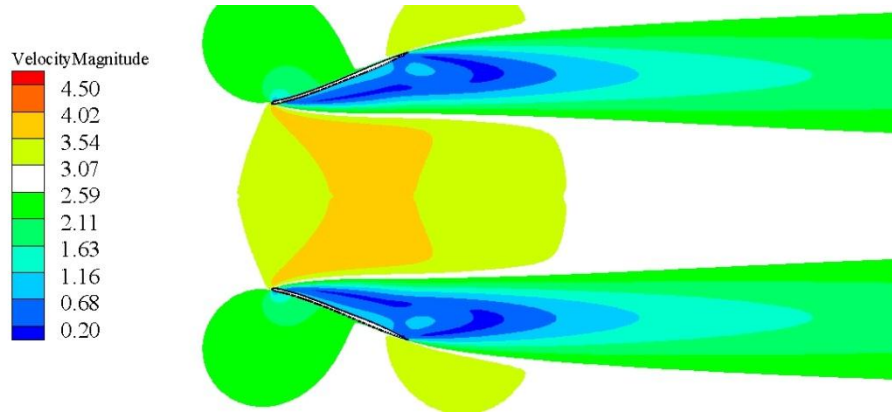
D_{15}

Figure 5. 6 Contours of Velocity Magnitude inside and around different diffuser
(where D_i represent no. of Diffuser)

5.2.2 Model Fitting and Validation

A quadratic response surface is developed showing the relationship between fluid velocity at the throat and 4 control points (design variables). The statistical software Minitab is used for this purpose. The desired regression model is given by

$$
\begin{aligned}
\text{Velocity} = \ & 3.23 - 0.01B - 0.07C - 0.18D + 0.55E - 0.02B^2 + 0.03C^2 - 0.01D^2 \\
& - 0.39E^2 + 0BC + 0.02BD + 0.01BE - 0.04CD + 0.04CE \\
& + 0.07DE \quad\quad\quad\quad\quad\quad\quad\quad\quad\quad\quad\quad\quad\quad\quad\quad\quad (5.1)
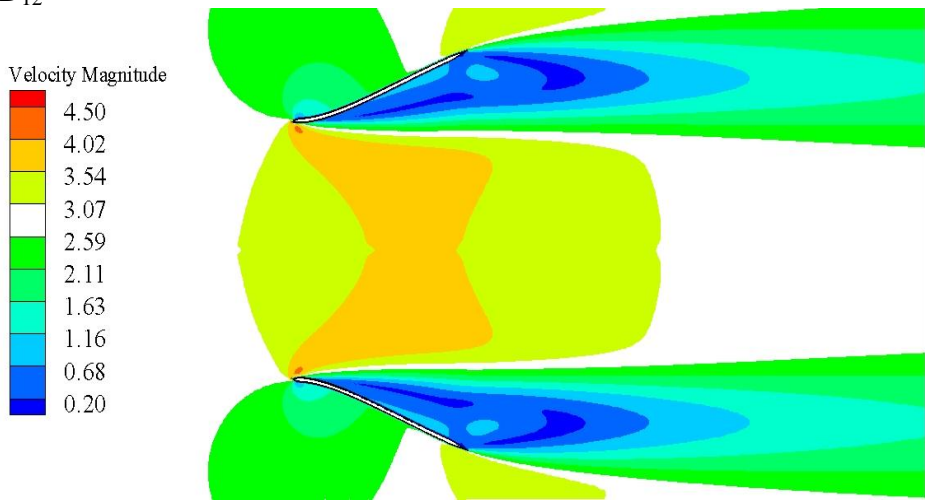\end{aligned}
$$

In above equation velocity is the depended variable (the response of the system) while B, C, D, E are the y-coordinates of 4 control points. The first point is fixed (A) its no variation along y-Axis so we didn't include in model. In order to validate the above mentioned statistical model, the flow inside the two new diffuser geometries $(D_{16} - D_{17})$ is simulated using both above mentioned response surface model and computational fluid dynamic techniques. The comparison of the predicted values of the fluid velocities is given in Table 5.5. It can be observed that the maximum difference between the two values is less than 5%.

60

Table 5.5 Velocity at diffuser throat calculated using CFD and response surface regression

Diffuser Geometries	Velocity at Throat Using CFD (m/s)	Velocity at Throat Using Regression Model (m/s)	Difference (%)
$D16$	3.28	3.24	0.057
D17	3.40	3.25	4.5

5.2.3 Optimization Analysis

The optimum set of input parameters producing the optimal response value is determined using response optimizer and response surface plots. Figure 5.7 is showing the effect of each factor on the response or composite desirability. Here the vertical red and horizontal blue lines represent the current settings and response values respectively. The values of composite desirability lie between 0 and 1 which corresponds to the undesirable and optimal performance for the studied factors response. So the maximum value of composite desirability is showing the occurrence optimal solution.

It can be observed from Figure 5.7 that the maximum velocity that can be achieved is 3.6751m/s. Hence by using optimum geometrical parameters for the diffuser, a velocity augmentation of 34.3 **%** can be achieved in comparison to baseline straight wall diffuser.

New D 0.73799	High Cur Low	a 0.0342 [0.0] 0.0	b 0.0685 [0.0] 0.0	c 0.1059 [0.0018] 0.0	d 0.1385 [0.1041] 0.0
Composite Desirability 0.73799					
Velocity Maximum y = 3.6751 d = 0.73799					
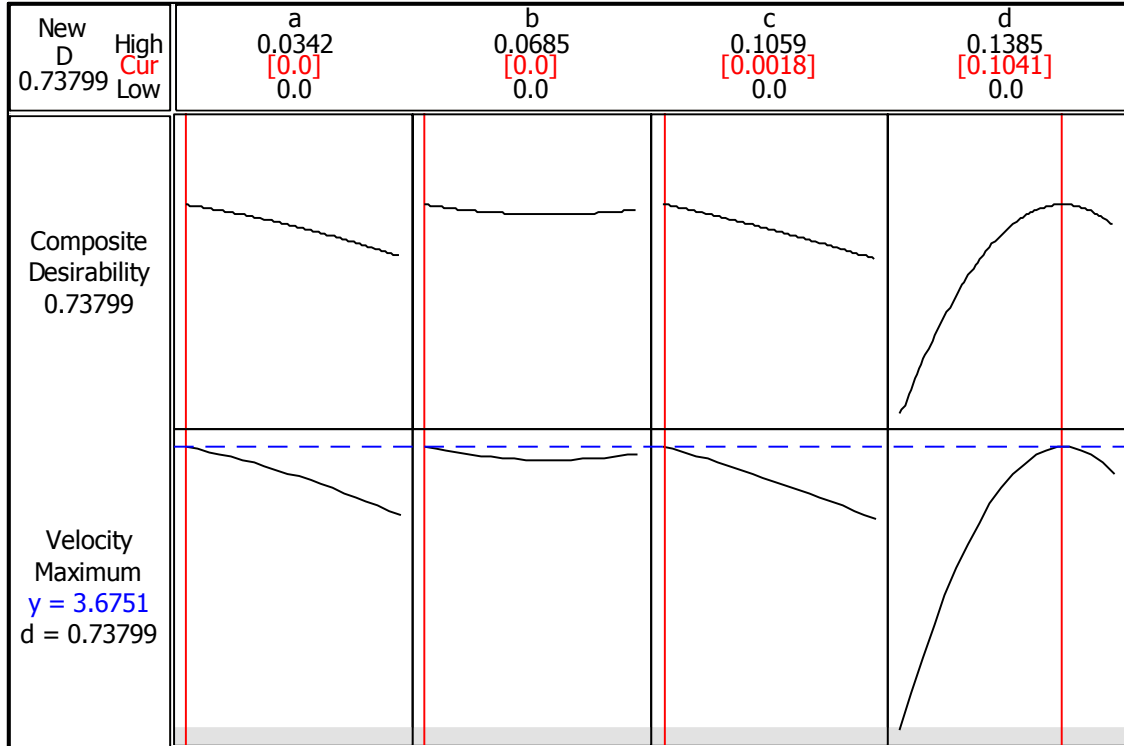
Figure 5. 7 Response optimizer for the optimum input parameters

5.3.   Performance Analysis of Optimized Diffuser

The performance of optimized diffuser is analyzed using numerical actuator disc approach. For this purpose, first the flow around the line projection representing the actuator disc is simulated. In the model setup, the line is assigned a fan boundary condition. The pressure drop across the whole line is defined using the following relation

$$C_t = \frac{P^+ - P^-}{0.5\ \rho U^2} \tag{5.2}$$

Here ρ is the density and U is free steam velocity. Two different approaches have been used to find the thrust co-efficient (C_t) i.e actuator disk and blade element method. The pressure distribution on the diffuser centerline is shown in Figure 5.8
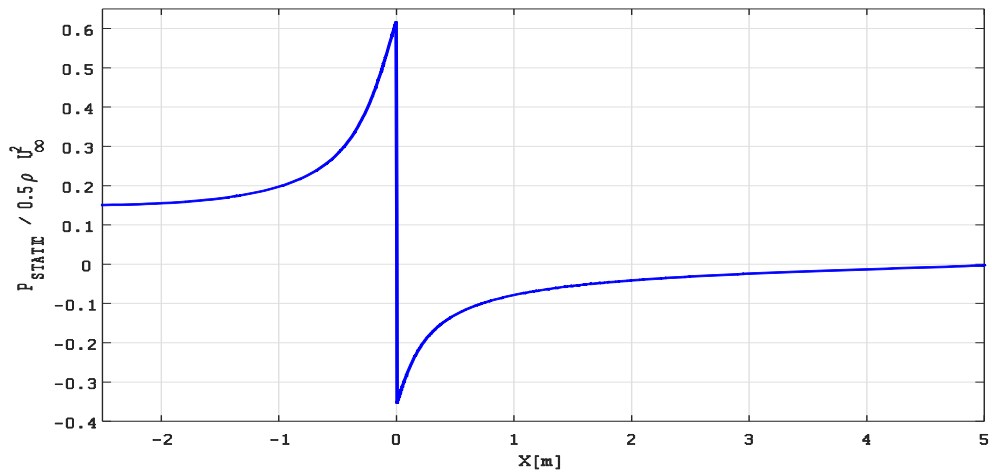
(a)
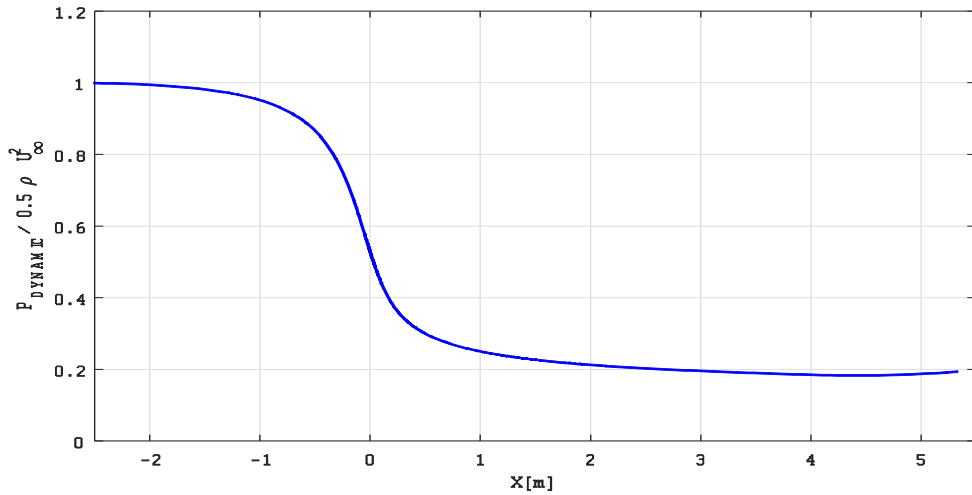
(b)

Figure 5. 8 Centerline Pressure distribution (a) Static Pressure (b) Dynamics Pressure

Contours of x component of velocity and gauge pressure are displayed in Figures 5.9 and 5.10 respectively. It can be observed from the Figure 5.9 that there is a reduction in velocity followed by the stream tube expansion due to the presence of disk. Similarly the pressure jump generated by disk is evident in Figures 5.10
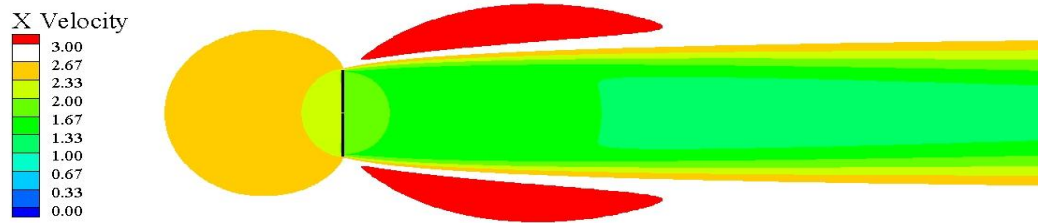
Figure 5. 9 Contours of X-Component of Velocity
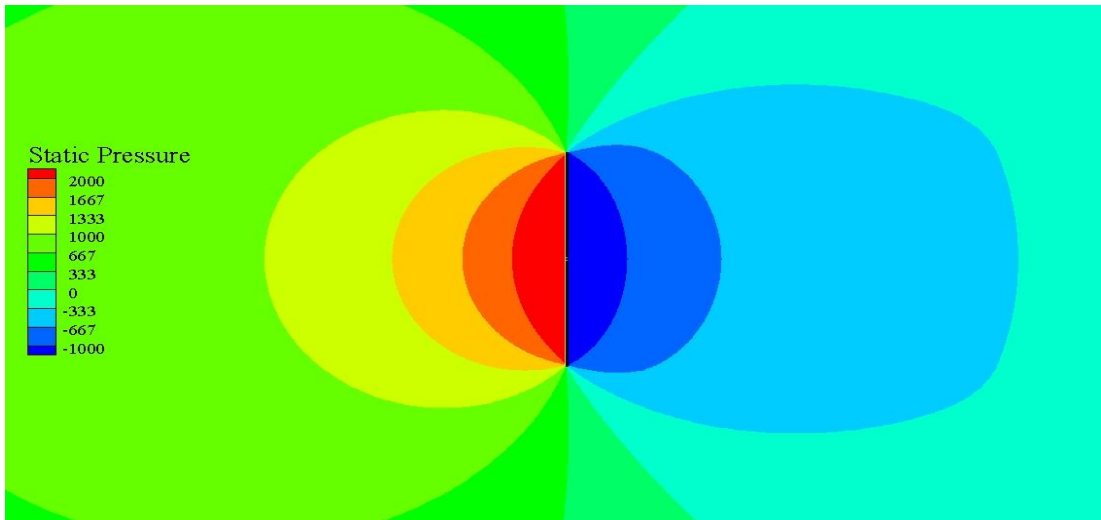
Figure 5. 10 Contours of Static Pressure

Figure **5.11** shows the effect of the presence of the diffuser in terms of flow augmentation at actuator disc. It can clearly be observed that the diffuser increases axial velocity, when compared to the bare actuator.
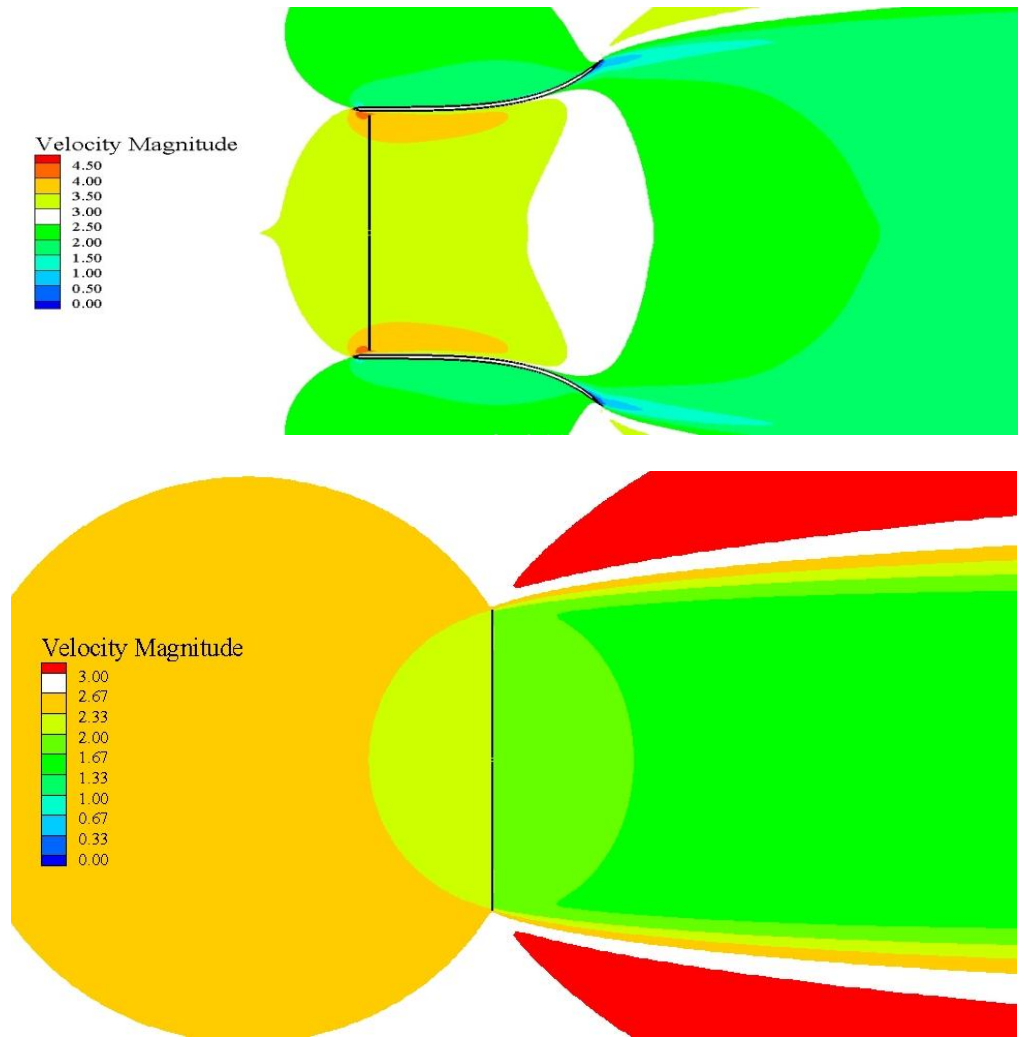
Figure 5. 11 Contours of velocity magnitude at actuator disk with and without diffuser

CHAPTER 6

Conclusions and Future Scope of Work

This chapter provides brief summary of conclusive results derived from the current research. Recommendations for future efforts are also suggested.

6.1 Conclusion

The aim of this research is the design and optimization of a diffuser for horizontal axis hydrokinetic turbine application. The main decisions pinched from the above research are following:

1. By finding the optimum set of input parameters, a velocity augmentation of 34.3% can be achieved in comparison to baseline diffuser.
2. The power output of the optimum diffuser is 131.28% more than that of the baseline diffuser.
3. The optimized curved diffuser produces more velocity augmentation as compared to the straight wall one having the same area ratio (outlet area/inlet area).

## 6.2 Future Work

Following are the main suggestions for the future work in the area of diffuser augmented tidal turbines.

1. The turbulence in the inflow effects the performance of diffuser augmented HAHT. The turbulence intensity (TI) is the most commonly used parameter to describe turbulence in marine energy applications. The impact of TI on diffuser augmented HAHT efficiency needs to be investigated.
2. Performance of diffuser augmented HAHT needs to be analyzed in different yaw operations using CFD techniques.
3. Optimization of rotor blade geometry for given diffuser will be the next step in the same area.

Bibliography

[1].   Pachauri, R.K.; Meyer, L.A. 2014 Climate Change : Synthesis Report, Publisher: IPCC, Geneva, Switzerland; pp. 2-26

[2].   Goldemberg, J., 2006. The promise of clean energy. Energy policy, 34(15), pp.2185-2190.

[3].   Sjolte, J., Tjensvoll, G. and Molinas, M., 2013. Power collection from wave energy farms. Applied Sciences, 3(2), pp.420-436.

[4].   Ning, D.Z., Zhao, X.L., Chen, L.F. and Zhao, M., 2018. Hydrodynamic performance of an array of wave energy converters integrated with a pontoon-type breakwater. Energies, 11(3), p.685.

[5].   Rahm, M., 2010. Ocean wave energy: underwater substation system for wave energy converters (Doctoral dissertation), Acta Universitatis Upsaliensis, Sweden.

[6].   Rusu, E. and Onea, F., 2018. A review of the technologies for wave energy extraction. Clean Energy, 2(1), pp.10-19.

[7].   Bryd.G., Naik, S., Fraenkel, P. and Bullen, C.R., 1998. Matching tidal current plants to local flow conditions. Energy, 23en, I (9), pp.699-709.

[8].   Bahaj, A.S. and Myers, L.E., 2003. Fundamentals applicable to the utilisation of marine current turbines for energy production. Renewable energy, 28(14), pp.2205-2211.

[9].   Chauhan, P., Patel, P. and Sheth, S., (NCIET-2015), Tidal Stream Turbine-Introduction, current and future Tidal power stations, National Conference on Innovative and Emerging Technologies (SRPEC, Unjha, Volume: 1, pp. 413-416

[10].   Goundar, J.N. and Ahmed, M.R., 2013. Design of a horizontal axis tidal current turbine. Applied energy, 111, pp.161-174.

[11].   Khalid, S.S., Liang, Z. and Shah, N., 2012. Harnessing tidal energy using vertical axis tidal turbine. Research Journal of Applied Sciences, Engineering and Technology, 5(1), pp.239-252.

[12]. Kinsey, T. and Dumas, G., 2012. Three-dimensional effects on an oscillating-foil hydrokinetic turbine. Journal of fluids engineering, 134(7), p.071105.

[13]. Buigues, G., Zamora, I., Mazón, A.J., Valverde, V. and Pérez, F.J., 2006, Sea energy conversion: problems and possibilities. In International Conference on Renewable Energies and Power Quality (ICREPQ'06), Palma de Mallorca, Spain, pp. 1-8.

[14]. Roberts, A., Thomas, B., Sewell, P., Khan, Z., Balmain, S. and Gillman, J., 2016. Current tidal power technologies and their suitability for applications in coastal and marine areas. Journal of Ocean Engineering and Marine Energy, 2(2), pp.227-245.

[15]. Olinger, D.J. and Wang, Y., 2015. Hydrokinetic energy harvesting using tethered undersea kites. Journal of Renewable and Sustainable Energy, 7(4), p.043114.

[16]. Etemadi, A., Emdadi, A., AsefAfshar, O. and Emami, Y., 2011. Electricity generation by the ocean thermal energy. Energy Procedia, 12, pp.936-943.

[17]. Vega, L.A., 2012. Ocean thermal energy conversion. Encyclopedia of Sustainability Science and Technology, pp.7296-7328.

[18]. Masutani, S.M. and Takahashi, P.K., 2001. Ocean thermal energy conversion (OTEC).Oceanography, 22(609), p.625.

[19]. Yip, N.Y., Brogioli, D., Hamelers, H.V. and Nijmeijer, K., 2016. Salinity gradients for sustainable energy: primer, progress, and prospects. Environmental science & technology, 50(22), pp.12072-12094.

[20]. He, Y., Huang, Z., Chen, B., Tsutsui, M., Miao, X.S. and Taniguchi, M., 2017. Electrokinetic Analysis of Energy Harvest from Natural Salt Gradients in Nanochannels. Scientific reports, 7(1), p.13156.

[21]. Ramon, G.Z., Feinberg, B.J. and Hoek, E.M., 2011. Membrane-based production of salinity-gradient power. Energy & environmental science, 4(11), pp.4423-4434.

[22]. Fraenkel, P.L., 2002. Power from marine currents. Proceedings of the Institution of Mechanical Engineers, Part A: Journal of Power and Energy, 216(1), pp.1-14.

[23]. Wang, J., Piechna, J., Gower, B. and Müller, N., 2011, January. Performance Analysis of Diffuser-Augmented Composite Marine Current Turbine Using CFD. In ASME 2011 5th International Conference on Energy Sustainability, Washington, DC, USA, pp. 1273-1278.

[24].   Lawn, C.J., 2003. Optimization of the power output from ducted turbines. Proceedings of the Institution of Mechanical Engineers, Part A: Journal of Power and Energy, 217(1), pp.107-117.

[25].   Setoguchi, T., Shiomi, N. and Kaneko, K., 2004. Development of two-way diffuser for fluid energy conversion system. Renewable Energy, 29(10), pp.1757-1771.

[26].   Kirke, B., 2006. Developments in ducted water current turbines. Tidal paper, pp. 1–13.

[27].   Munch, C.; Vonlanthen, M.; Gomes, J.; Luquet, R.; Guinard, P.; Avellan, F. Design and Performance Assessment of a Tidal Ducted Turbine. 2009 In proceedings of the 3rd IAHR International Meeting of the Workgroup on Cavitation and Dynamic Problems in Hydraulic Machinery and Systems, Brno, Czech Republic,

[28].   Gaden, D.L. and Bibeau, E.L., 2010. A numerical investigation into the effect of diffusers on the performance of hydro kinetic turbines using a validated momentum source turbine model. Renewable Energy, 35(6), pp.1152-1158.

[29].   Shives, M. and Crawford, C., 2010, October. Computational analysis of ducted turbine performance. In 3rd International Conference on ocean energy, Bilbao, Spain. (Vol. 6). pp.1-6

[30].   Scherillo, F., Maisto, U., Troise, G., Coiro, D.P. and Miranda, S., 2011, June. Numerical and experimental analysis of a shrouded hydroturbine. In International conference on clean electrical power (ICCEP) Ischia, Italy. pp. 216-222.

[31].   Reinecke, J. and Venter, G., 2011. Effect of a Diffuser on the Performance of an Ocean Current Turbine, (Master's dissertation), university of Stellenbosch, South Africa.

[32].   Sun, H. and Kyozuka, Y., 2012. Experimental validation and numerical simulation evaluation of a shrouded tidal current turbine. Journal of the Japan Society of Naval Architects and Ocean Engineers, 16, pp.25-32.

[33].   Mehmood, N., Z.L. and Khan, J., 2012. CFD study of NACA 0018 for diffuser design of tidal current turbines. Research Journal of Applied Science, Engineering and Technology, 4(21), pp.4552-4560.

[34].   Shi, W., Wang, D., Atlar, M., Guo, B. and Seo, K.C., 2015. Optimal design of a thin-wall diffuser for performance improvement of a tidal energy system for an AUV. Ocean Engineering, 108, pp.1-9.

[35].   Khunthongjan, P. and Janyalertadun, A., 2012. A study of diffuser angle effect on ducted water current turbine performance using CFD. Songklanakarin J. Sci. Technol., 34(1), pp. 61–67.

[36].   Shinomiya, L.D., Aline, D., Maria, A., Felamingo, T., Gustavo, J., Amarante, A.L. and Pinheiro, J.R., 2013, November. Numerical Study of Flow around Diffusers with Different Geometry Using CFD Applied to Hydrokinetics Turbines Design. In OBEM International congress of Mechanical Engineering, Ribeirão Preto, Brazil. (Vol. 7). pp. 1033–1040

[37].   Ait-Mohammed, M., Tarfaoui, M. and Laurens, J.M., 2014, April. Predictions of the hydrodynamic performance of horizontal axis marine current turbines using a panel method program. In International Conference on Renewable Energies and Power Quality, Córdoba, Spain, pp. 386-391.

[38].   Ponta, F.L. and Jacovkis, P.M., 2008. Marine-current power generation by diffuser-augmented floating hydro-turbines. Renewable energy, 33(4), pp.665-673.

[39].   Chen, H. and Zhou, D., 2014. Hydrodynamic numerical simulation of diffuser for horizontal axis marine current turbine based on CFD. In IOP Conference Series: Earth and Environmental Science (Vol. 22, No. 6, p. 062001). IOP Publishing.

[40].   Shahsavarifard, M., Bibeau, E.L. and Chatoorgoon, V., 2015. Effect of shroud on the performance of horizontal axis hydrokinetic turbines. Ocean Engineering, 96, pp.215-225.

[41].   Ponta, F.L. and Jacovkis, P.M., 2008. Marine-current power generation by diffuser-augmented floating hydro-turbines. Renewable energy, 33(4), pp.665-673.

[42].   Jo, C.H., Kim, D.Y., Hwang, S.J. and Goo, C.H., 2016. Shape Design of the Duct for Tidal Converters Using Both Numerical and Experimental Approaches (pre-2015). Energies, 9(3), p.185.

[43].   Elbatran, A.H., Yaakob, O., Ahmed, Y. and Abdallah, F., 2016. Augmented diffuser for horizontal Axis marine current turbine. International Journal of Power Electronics and Drive Systems (IJPEDS), 7(1), pp.235-245.

[44].   Gaden, D.L. and Bibeau, E.L., 2010. A numerical investigation into the effect of diffusers   on the performance of hydro kinetic turbines using a validated momentum source turbine   model. Renewable Energy, 35(6), pp.1152-1158.

[45].   Ponta, F.L. and Jacovkis, P.M., 2008. Marine-current power generation by diffuser-augmented floating hydro-turbines. Renewable energy, 33(4), pp.665-673.

[46].   Riglin, J., Schleicher, W.C. and Oztekin, A., 2014, November. Diffuser Optimization for a Micro-Hydrokinetic Turbine. In ASME 2014 International Mechanical Engineering Congress and Exposition, American Society of Mechanical Engineers, pp. 17.

[47].   Shahsavarifard, M., Bibeau, E.L. and Chatoorgoon, V., 2015. Effect of shroud on the performance of horizontal axis hydrokinetic turbines. Ocean Engineering, 96, pp.215-225.

[48].   Cresswell, N.W., Ingram, G.L. and Dominy, R.G., 2015. The impact of diffuser augmentation on a tidal stream turbine. Ocean Engineering, 108, pp.155-163.

[49].   Shives, M.R., 2011. Hydrodynamic modeling, optimization and performance assessment for ducted and non-ducted tidal turbines (Doctoral dissertation), University of Victoria , Canada.

[50].   Shives, M. and Crawford, C., 2012. Developing an empirical model for ducted tidal turbine performance using numerical simulation results. Proceedings of the Institution of Mechanical Engineers, Part A: Journal of Power and Energy, 226(1), pp.112-125.

[51].   Shi, W., Wang, D., Atlar, M., Guo, B. and Seo, K.C., 2015. Optimal design of a thin-wall diffuser for performance improvement of a tidal energy system for an AUV. Ocean Engineering, 108, pp.1-9.

[52].   Fleming, C.F. and Willden, R.H., 2016. Analysis of bi-directional ducted tidal turbine performance. International journal of marine energy, 16, pp.162-173.

[53].   Scherillo, F., Maisto, U., Troise, G., Coiro, D.P. and Miranda, S., 2011, June. Numerical and experimental analysis of a shrouded hydroturbine. In International conference on clean electrical power (ICCEP) (pp. 216-222).

[54].   Sun, H. and Kyozuka, Y., 2012. Experimental validation and numerical simulation evaluation of a shrouded tidal current turbine. Journal of the Japan Society of Naval Architects and Ocean Engineers, 16, pp.25-32.

[55].   Belloni, C.S., Willden, R.H. and Houlsby, G.T., 2013. A numerical analysis of bidirectional ducted tidal turbines in yawed flow. Marine Technology Society Journal, 47(4), pp.23-35.

[56].   Riglin, J.D., 2016. Design, Modeling, and Prototyping of a Hydrokinetic Turbine Unit for River Application, Lehigh University, Pennsylvania, USA.

[57].   Versteeg, H.K. and Malalasekera, W., 2007. An introduction to computational fluid dynamics: the finite volume method. Pearson Education.

[58].   Gerber, A. G., Jeans, T., Culina, J. and Holloway, A. G. L. (2013), Turbulent tidal flow in Minas Passage using high fidelity CFD simulation, in `Proc. 10th European Wave and Tidal Energy Conference'.

[59].   Moin, P. and Mahesh, K., 1998. Direct numerical simulation: a tool in turbulence research. Annual review of fluid mechanics, 30(1), pp.539-578.

[60].   Pope, S. B., 2001. Turbulent Flows. Cambridge University Press, pp 387-452.

[61].   Kostić, Č., 2015. Review of the Spalart-Allmaras turbulence model and its modifications to three-dimensional supersonic configurations. Scientific Technical Review, 65(1), pp.43-49.

[62].   Sørensen, J.N., 2016. General momentum theory for horizontal axis wind turbines (Vol. 4). Switzerland: Springer.

[63].   Mahmuddin, F. 2017 Rotor Blade Performance Analysis with Blade Element Momentum Theory. Energy Procedia 105: p. 1123-1129.

[64].   Chitale, K.C., Rasquin, M., Sahni, O., Shephard, M.S. and Jansen, K.E., 2014. Boundary layer adaptivity for incompressible turbulent flows. 11th World Congress on Computational Mechanics (WCCM XI) 5th European Conference on Computational Mechanics (ECCM V) 6th European Conference on Computational Fluid Dynamics (ECFD VI), Barcelona 2014, pp1-21

[65].   Roache, P.J. Perspective: a method for uniform reporting of grid refinement studies. J Fluid Eng, 1994,116, 405-413, doi:10.1115/1.2910291

[66].   Celik, I. B.; Ghia, U.; Roache, P.J. 2008, Procedure for estimation and reporting of uncertainty due to discretization in CFD applications. J Fluid Eng, 130, 1-4, doi: 10.1115/1.2960953

[67].   Gabriel, E.T.; Mueller, T.J. 2004 Low-aspect-ratio wing aerodynamics at low Reynolds number. AIAA Journal, , 42, 865-873, doi: 10.2514/1.439

[68].   Cosyn, P.H.; Vierendeels, J. 2006 Numerical investigation of low-aspect-ratio wings at low Reynolds numbers. J Aircraft, , 43, 713-722, doi: 10.2514/1.16991.

[69].   Samareh, J. A. A 1999.Survey of Shape Parameterization Techniques. CEAS/AIAA/ICASE/NASA Langley International Forum on Aeroelasticity and Structural Dynamics, Williamsburg, United States,

[70].   Derksen, R.W.; Rogalsky T. Bezier-PARSEC: 2010. An optimized aerofoil parameterization for design. Adv Eng Softw., , 41, 923-930, doi: 10.1016/j.advengsoft.2010.05.002